

1 Occurrence and characteristics of 2 mesoscale eddies in the tropical 3 northeast Atlantic Ocean

4 **F. Schütte**¹, **P. Brandt**^{1,2} and **J. Karstensen**¹

5 [1] GEOMAR Helmholtz Centre for Ocean Research Kiel, Kiel, Germany

6 [2] Christian-Albrechts-Universität zu Kiel, Kiel, Germany

7 Correspondence to: F. Schütte (fschuette@geomar.de)

8 **Abstract**

9 Coherent mesoscale features (referred to here as eddies) in the tropical northeast Atlantic
10 (between 12°N - 22°N and 15°W - 26°W) are examined and characterised. The eddies'
11 surface signatures are investigated using 19 years of satellite derived sea level anomaly (SLA)
12 data. Two automated detection methods are applied, the geometrical method based on closed
13 streamlines around eddy cores, and the Okubo-Weiß method based on the relation between
14 vorticity and strain. Both methods give similar results. Mean eddy surface signatures of SLA,
15 sea surface temperature (SST) and salinity (SSS) anomalies are obtained from composites of
16 all snapshots around identified eddy cores. Anticyclones/cyclones are identified by an
17 elevation/depression of SLA and enhanced/reduced SST and SSS in its cores. However, about
18 20% of all anticyclonically rotating eddies show reduced SST and reduced SSS instead. These
19 kind of eddies are classified as anticyclonic mode-water eddies (ACMEs). About 146 ± 4
20 eddies per year with a minimum lifetime of 7 days are identified (52% cyclones, 39%
21 anticyclones, 9% ACMEs) with rather similar mean radii of about 56 ± 12 km. Based on
22 concurrent in-situ temperature and salinity profiles (from Argo float, shipboard and mooring
23 data) taken inside of eddies, distinct mean vertical structures of the three eddy types are
24 determined. Most eddies are generated preferentially in boreal summer and along the West
25 African coast at three distinct coastal headland regions and carry South Atlantic Central
26 Water supplied by the northward flow within the Mauretania coastal current system.
27 Westward eddy propagation (on average about 3.00 ± 2.15 km d⁻¹) is confined to distinct
28 zonal corridors with a small meridional deflection dependent on the eddy type (anticyclones –
29 equatorward, cyclones – poleward, ACMEs – no deflection). Heat and salt fluxes out of the

- 1 coastal region and across the Cap Verde Frontal Zone, which separates the shadow zone from
- 2 the ventilated subtropical gyre, are calculated.

1 **1 Introduction**

2 The generation of eddies in coastal upwelling regions is strongly related to the eastern
3 boundary circulation and its seasonal variations. Within the tropical Atlantic Ocean off
4 northwest Africa (TANWA; 12°N to 22°N and 26°W to 15°W), the large-scale surface
5 circulation responds to the seasonal variability of the trade winds and the north/south
6 migration of the Intertropical Convergence Zone (ITCZ) (e.g. Stramma and Isemer (1988),
7 Siedler et al. (1992), Stramma and Schott (1999)). The seasonal wind pattern results in a
8 strong seasonality of the flow field along the northwest African coast and in coastal upwelling
9 of different intensity. The coastal upwelling in the TANWA is mainly supplied by water
10 masses of South Atlantic origin (Jones and Folkard (1970), Hughes and Burton (1974),
11 Wooster et al. (1976), Mittelstaedt (1991), Ould-Dedah et al. (1999), Pastor et al. (2008),
12 Glessmer et al. (2009), Peña - Izquierdo et al. (2015)), which are relatively cold and fresh
13 compared to the North Atlantic waters further offshore. The water mass transition region
14 coincides with the eastern boundary shadow zone, where diffusive transport pathways
15 dominate (Luyten et al., 1983) with weak zonal current bands superimposed (Brandt et al.,
16 2015). The oceanic circulation in the TANWA is most of the time weak and the velocity field
17 is dominated by cyclonic and anticyclonic eddies. However, global as well as regional
18 satellite based studies of eddy distribution and characterisation (Chelton et al. (2007),
19 Chaigneau et al. (2009), Chelton et al. (2011)) found high eddy activity in terms of eddy
20 generation in the TANWA, but only rare occurrence of long-lived eddies (>112 days referred
21 to Chelton et al. (2007), >35 days, referred to Chaigneau et al. (2009)). Karstensen et al.
22 (2015) studied individual energetic eddy events based on a combination of in-situ and satellite
23 based Sea Level Anomaly (SLA) data, and reported eddy life times of more than 200 days in
24 the TANWA region. These individual eddies carried water mass characteristics typical for the
25 shelf region up to 900 km off the African coast. One possible generation area for such eddies
26 is the Cap-Vert headland at about 14.7°N near the Senegalese coast (Karstensen et al., 2015).
27 Analysing surface drifter data and high-resolution satellite data, Alpers et al. (2013) described
28 the evolution of an energetic sub-mesoscale eddy at the Cap-Vert headland that was
29 presumably generated by flow separation of a wind-forced coastal jet. Earlier studies reported
30 on the importance of eddy transport in the TANWA region (e.g. Hagen (1985); Barton
31 (1987); Zenk et al. (1991)). However, characteristics of the eddy field in the TANWA region
32 such as seasonality in eddy generation, eddy lifetime, vertical structure, or frequency of
33 occurrence are so far undocumented.

1 More comprehensive information on eddy dynamics was gained for the Pacific Ocean eastern
2 boundary upwelling systems. The eddy generation in the northeast Pacific Ocean, off
3 California and Mexico including the California Current System was studied with high-
4 resolution models applied to reproduce observed characteristics of the eddy field (Liang et al.
5 (2012), Chang et al. (2012)). These studies highlight hotspots of eddy generation associated
6 with local wind fluctuations (e.g. over the Gulf of Tehuantepec and Papagayo), but also
7 suggest an important role of low-frequency wind and boundary forcing. For the southeast
8 Pacific Ocean, off Peru and Chile, including the Peru-Chile Current System, Chaigneau et al.
9 (2008) and Chaigneau et al. (2011) analysed the seasonal to interannual variability of eddy
10 occurrence as well as the mean vertical structure of eddies based on Argo floats.

11 A schematic of the current system of the TANWA in boreal spring and in boreal autumn is
12 presented in Figure 1. In the north of the TANWA the Canary Current (CC) transports cold
13 water southwards along the African shelf. It detaches from the coast around Cap Blanc (more
14 specifically at about 20°N during spring and 25°N during autumn) and joins the North
15 Equatorial Current (NEC) (Mittelstaedt (1983), Mittelstaedt (1991)). The dominant feature
16 south of the TANWA is the eastward flowing North Equatorial Countercurrent (NECC)
17 extending over a latitudinal range from 3°N to about 10°N. It has a pronounced seasonal cycle
18 with maximum strength in boreal summer and autumn, when the ITCZ reaches its
19 northernmost position. During that period the NECC is a continuous zonal flow across the
20 entire tropical Atlantic (e.g. Garzoli and Katz (1983), Richardson and Reverdin (1987),
21 Stramma and Siedler (1988), Polonsky and Artamonov (1997)). When approaching the
22 African coast, the current is partly deflected to the north feeding a sluggish northward flow
23 along the coast. This current is referred to as Mauretania Current (MC) and reaches latitudes
24 up to 20°N (Mittelstaedt, 1991). The strength of the MC is strongly related to the seasonally
25 varying NECC with a time lag of one month (Lázaro et al., 2005). During boreal winter and
26 spring when the NECC is pushed to the equator and becomes unstable, the MC becomes weak
27 and unsteady and only reaches latitudes south of Cap Vert (Mittelstaedt (1991), Lázaro et al.
28 (2005)). During this period the wind induced coastal upwelling is at its maximum.
29 Simultaneously, the large-scale pressure gradient set by the southward winds induces an
30 along-slope subsurface current, known as Poleward Undercurrent (PUC) (Barton, 1989).
31 During boreal summer the MC re-establishes contemporaneously to the suppression of coastal
32 upwelling south of Cap Blanc at 21°N (Peña-Izquierdo et al., 2012).

33 The eastern boundary upwelling is supplied by waters of South Atlantic origin through a
34 pathway consisting of the North Brazil Current (NBC), the North Equatorial Undercurrent

1 (NEUC) and the PUC. Hence, the purest South Atlantic Central Water (SACW) within the
2 TANWA is found close to the coast (Figure 2), while further offshore a transition towards the
3 more saline and warmer North Atlantic Central Water (NACW) is observed. The boundary
4 between the regimes is associated with the Cape Verde Frontal Zone (CVFZ, Figure 2),
5 characterized by a sharp horizontal salinity gradient of 0.9 per 10km (Zenk et al., 1991). The
6 efficiency of mesoscale eddies to transport cold and less saline SACW from their generation
7 regions near the coast into the open ocean where NACW dominates is one topic investigated
8 in this paper. In particular, the characteristics of these eddies (size, structure, frequency) and
9 their potential role in the transport of heat and salt will be examined in more detail.

10 The paper is organized as follows: In section 2, the different data types (satellite derived and
11 in-situ) will be introduced as well as the techniques to automatically detect and track eddies
12 from satellite data and to derive their vertical structure. In section 3 the eddy characteristics
13 (origin, pathways, surface signature) and statistics (frequency) are discussed and the temporal
14 and spatial variability of eddy generation and eddy pathways are examined. The mean
15 horizontal and vertical eddy structures are derived and, in combination with the eddy
16 statistics, used to estimate the transport of volume, heat and salt from the shelf region into the
17 open ocean. Finally our results are summarized in section 4.

18 **2 Data and Methods**

19 **2.1 Satellite data**

20 **2.1.1 SLA, SST and SSS**

21 The delayed-time reference dataset “all-sat-merged” of SLA (Version 2014), which is used in
22 the study, is produced by Ssalto/Duacs and distributed by AVISO (Archiving, Validation, and
23 Interpretation of Satellite Oceanographic), with support from CNES
24 [<http://www.aviso.altimetry.fr/duac/>]. The data is a multi-mission product, mapped on a $1/4^\circ$
25 $\times 1/4^\circ$ Cartesian grid and has a daily temporal resolution. The anomalies are computed with
26 respect to a twenty-year mean. Data for the period January 1995 to December 2013 are
27 considered here. Geostrophic velocity anomalies derived from the SLA provided by AVISO
28 for the same timespan are also used in this study. Given the interpolation technique applied to
29 the along track SLA data Gaussian shaped eddies with a radius $> \sim 45$ km can be detected;
30 eddies of smaller diameter may be detected but their energy is damped (Fu and Ferrari, 2008).

31

1 For SST the dataset “Microwave Optimally interpolated Sea Surface Temperature” from
2 Remote Sensing Systems (www.remss.com) is used. It is derived from satellite microwave
3 radiometers, which have the capability to measure through clouds. It has a 25 km resolution
4 and contains the SST measurements from all operational radiometers for a given day. All OI
5 SST values are corrected using a diurnal model to create a foundation SST that represents a
6 12-noon temperature [www.remss.com]. Daily data from the outset January 1, 1998 to
7 December 31, 2013 is used here and mapped similar to the SLA data on a $1/4^\circ \times 1/4^\circ$
8 Cartesian grid.

9
10 Our study also includes sea surface salinity (SSS) data. We make use of the LOCEAN_v2013
11 SSS product available from January 1, 2010 until the end of our analysis period (December
12 31, 2013). The data is distributed by the Ocean Salinity Expertise Center (CECOS) of the
13 CNES-IFREMER Centre Aval de Traitement des Donnees SMOS (CATDS), at IFREMER,
14 Plouzane (France). The data is created using the weight averaging method described in Yin et
15 al. (2012) and the flag sorting described in Boutin et al. (2013). Finally the data is mapped on
16 a $1/4^\circ \times 1/4^\circ$ Cartesian grid and consist of 10-day composites.

18 **2.1.2 Eddy identification and tracking from satellite data**

19 In order to detect eddy-like structures two different methods are applied to the SLA data. The
20 first method, the Okubo-Weiß-Method (OW-method; Okubo (1970), Weiss (1991)), has been
21 frequently used to detect eddies using satellite data as well as the output from numerical
22 studies (e.g. Isern-Fontanet et al. (2006), Chelton et al. (2007), Sangrà et al. (2009)). The
23 basic assumption behind the OW-method is that regions, where the relative vorticity
24 dominates over the strain, i.e. where rotation dominates over deformation, characterize an
25 eddy. In order to separate strong eddies from the weak background flow field a threshold
26 needs to be identified. For this study the threshold is set to $W_0 = -0.2 \cdot \sigma$, where σ is the
27 spatial standard derivation of the Okubo-Weiß parameter $W = s_n^2 + s_s^2 - \omega^2$. Here,
28 $s_n = \frac{\partial u}{\partial x} - \frac{\partial v}{\partial y}$ is the normal strain, $s_s = \frac{\partial v}{\partial x} + \frac{\partial u}{\partial y}$ is the shear strain and $\omega = \frac{\partial v}{\partial x} - \frac{\partial u}{\partial y}$ is the
29 relative vorticity. A similar definition of the threshold was used in other eddy studies applying
30 the OW-method (e.g. Chelton et al. (2007)). The maximum (minimum) SLA marks the eddy
31 center.

32 The second method for eddy detection is based on a geometric approach (GEO-method)
33 analyzing the streamlines of the SLA derived geostrophic flow. An eddy edge is defined as
34 the streamline with the strongest swirl velocity around a center of minimum geostrophic

1 velocity (Nencioli et al., 2010). For the detection of an eddy the algorithm requires two
 2 parameters a and b to be defined. The first parameter, a , is a search radius in grid points.
 3 Inside the search radius, the velocity reversal across the eddy center is identified (v
 4 component on an east-west section, u component on a north-south section). The second
 5 parameter, b , is used to identify the point of minimum velocity within a region that extends up
 6 to b grid points (for a more detailed description of the method see Nencioli et al. (2010)).
 7 After a few sensitivity tests in comparison with the results of the OW-method and following
 8 the instructions of Nencioli et al. (2010), we set $a=3$ and $b=2$. Optimal results were obtained
 9 when we linearly interpolated the AVISO velocity fields onto a 1/6 by 1/6 degree grid before
 10 we applied the algorithm (for more information see also Liu et al. 2012). If an eddy is
 11 detected an eddy center is identified analog to the OW-method as maximum (anticyclone) or
 12 minimum (cyclone) of SLA within the identified eddy structure.

13

14 When applying the two different eddy detection methods to the SLA data from the TANWA
 15 region, we used the same eddy detection thresholds for both methods, i.e. a feature only
 16 counts as an eddy, if its radius is larger than 45 km and it is detectable for a period of more
 17 than 7 days. Note, as the identified eddy areas are rarely circular we used the circle-equivalent
 18 of the area of the detected features to estimate the radius. For eddy tracking both eddy
 19 detection methods use the same tracking algorithm. An eddy trajectory was calculated if an
 20 eddy with the same polarity was found at least in 7 consecutive SLA maps (corresponding to
 21 one weeks) within a search radius of up to 50 km. Due to e.g. errors in SLA mappings
 22 (insufficient altimetric coverage) an eddy could vanish and reemerge after a while. Therefore
 23 we searched in 14 consecutive SLA maps (corresponding to 2 weeks) in a search radius of up
 24 to 100 km after an eddy disappearance, if eddies with the same polarity reemerges. If more
 25 than one eddy with the same polarity emerge within the search radius, we defined the
 26 following similarity parameter to discriminate between these eddies:

27

$$28 \quad X = \sqrt{\left(\frac{distance}{100}\right)^2 + \left(\frac{\Delta radius}{radius_0}\right)^2 + \left(\frac{\Delta vorticity}{vorticity_0}\right)^2 + \left(\frac{\Delta EKE}{EKE_0}\right)^2}, \quad (1)$$

29 which include four terms based on the distance between the disappeared and newly emerged
 30 eddies and the difference of their radii, mean vorticities and mean eddy kinetic energy (EKE).
 31 $Radius_0$, $vorticity_0$ and EKE_0 are the mean radius, vorticity and EKE of all identified
 32 eddies in TANWA. The newly emerged eddy with the smallest X is selected to be the same
 33 eddy. To give an idea of the uncertainty related to the detection technique both methods are

1 applied to the data. Every step is computed separately with both methods and the results are
2 compared.

3

4 **2.1.3 Eddy classification and associated mean spatial surface pattern**

5 From the geostrophic velocity data anticyclones (cyclones) can be identified due to their
6 negative (positive) vorticity. In the SLA data anticyclones (cyclones) are associated with a
7 surface elevation (depression). The maximum (minimum) SLA marks the eddy center. In
8 general, anticyclones (cyclones) carry enhanced (reduced) SST and enhanced (reduced) SSS
9 in their cores, respectively. However, we found that 20% of all detected anticyclones had cold
10 anomalies in their cores and a reduced SSS. This kind of eddies is classified as anticyclonic
11 mode-water eddies (ACMEs) or intrathermocline eddies (Kostianoy and Belkin, 1989) as will
12 later be confirmed when considering the in-situ observations (see below). Given that ACMEs
13 show distinct characteristics, which are contrasting to anticyclones (see below), we
14 distinguish in the following three types of eddies: anticyclones, cyclones and ACMEs.

15 Composites of satellite derived SST and SSS anomalies with an extent of 300 km x 300 km
16 around the eddy centers yield the mean spatial eddy surface pattern of temperature and
17 salinity for the respective eddy type. The information whether an eddy is cold/warm or
18 fresh/saline in the core is obtained by subtracting the average value over the edge of the box
19 from the average value over the eddy center and its closest neighboring grid points. To
20 exclude large-scale variations in the different datasets, the SST and SSS fields are low-pass
21 filtered with cutoff wavelength of 15° longitude and 5° latitude. Thereafter the filtered
22 datasets are subtracted from the original datasets thus preserving the mesoscale variability.
23 The composite plots are based only on eddies with a radius between 45-70 km and an absolute
24 SLA difference between the eddy center and the mean along the edge of the 300 km x 300 km
25 box used for the composites greater than 2 cm.

26

27 **2.2 In-situ Data**

28 **2.2.1 Argo Floats**

29 A set of irregular distributed vertical CTD profiles was obtained from the autonomous
30 profiling floats of the Argo program. The freely available data was downloaded from the
31 Global Data Assembly Centre in Brest, France (www.argodatamgt.org) and encompasses the

1 period from July 2002 to December 2013. Here only pressure (P), temperature (T) and salinity
2 (S) data flagged with Argo quality category 1 are used. The given uncertainties are ± 2.4 dbar
3 for pressure, ± 0.002 °C for temperature and ± 0.01 for uncorrected salinities. In most cases the
4 salinity errors are further reduced by the delayed-mode correction. For this analysis an
5 additional quality control is applied in order to eliminate spurious profiles and to ensure good
6 data quality in the upper layers. In the following, we give the criteria applied to the Argo float
7 profiles and in brackets the percentage, to which the criteria were fulfilled. Selected profiles
8 must i) include data between 0 and 10 m depth (98.2%), ii) have at least 4 data points in the
9 upper 200 m (98.8%), iii) reach down to 1000 m depths (95%), iv) continuous and consistent
10 temperature, salinity and pressure data (78%). This procedure reduced the number of profiles
11 by around 30% to 2022 Argo float profiles for the TANWA.

12

13 **2.2.2 Shipboard measurements**

14 In-situ CTD profile data collected during 20 ship expeditions to the TANWA within the
15 framework of different programs is used (Figure 2b; see Table 1 for further details). In total
16 579 profiles were available taken within the TANWA during the period March 2005 to June
17 2013. Data sampling and quality control followed the standards set by GO-SHIP (Hood et al.,
18 2010). However, we assume a more conservative accuracy of our shipboard data of about
19 twice the GO-SHIP standard, which is ± 0.002 °C and ± 0.004 for temperature and salinity,
20 respectively.

21

22 **2.2.3 CVOO Mooring**

23 The third set of in-situ data stems from the Cape Verde Ocean Observatory (CVOO) mooring.
24 The CVOO mooring is a deep-sea mooring deployed at a depth of about 3600 m, 60 km
25 northeast of the Cape Verdean island of São Vicente (Figure 2b). The nominal mooring
26 position is 17°36'N, 24°15'W. The mooring was first deployed in June 2006 and has been
27 redeployed in March 2008, October 2009, May 2011 and October 2012. Temperature and
28 salinity measurements in the upper 400 m have been typically recorded at depth of 30 m, 50
29 m, 70 m, 100 m, 120 m, 200 m, 300 m and 400 m using MicroCAT instruments. Data
30 calibration is done against shipboard CTD data during the service cruises. The uncertainties
31 are ± 0.002 °C for temperature and ± 0.01 for salinity.

32 The eddy detection methods identifies 22 eddies passing the CVOO mooring. For these eddy
33 events, the original time series with a temporal resolution of 15 or 20 minutes were low-pass
34 filtered with a cut-off period of 24 hours and consecutively subsampled to 1-day values in

1 order to reduce instrument noise and to match the resolution of the SLA maps. In total 429
2 profiles could be obtained. T/S anomaly profiles were derived as the difference of profiles
3 inside and outside of the eddies. The outside profiles were taken shortly before the eddy
4 passage.

5

6 **2.3 Determining the vertical structure of eddies detected in SLA data**

7 In order to investigate the vertical structure of eddies identified in SLA data a combination of
8 all available in-situ data sets was used. We had a total of 3030 CTD profiles available for the
9 time period 2002 to 2013, with about 67% Argo float profiles, 19% shipboard CTD profiles
10 and 14% mooring-based profiles (Figure 3). All profiles were vertically interpolated or re-
11 gridded to 1 m vertical resolution in the depth range 5 to 1000 m. Missing data points within
12 the first few meters of the water column were filled by constant extrapolation. For each
13 profile, we determined the mixed layer depth (MLD) as the depth where the in-situ
14 temperature decreased by 0.2 °C relative to 10m depth (de Boyer Montégut et al., 2004).

15 By co-location, in space and time, of eddies, that are identified in the SLA data using a
16 combination of the OW and the GEO-method (an eddy has to be identified by both
17 algorithms), with the combined in-situ data set, the vertical structures of anticyclones and
18 ACMEs (positive SLA) and cyclones (negative SLA) were assessed (Figure 4). The
19 classification results in 675 profiles taken in anticyclones/ACMEs, 499 profiles taken in
20 cyclones and 1856 profiles taken outside of detected eddies. Excluding the mooring based
21 profiles, from which we only extracted eddy events, around ~29% of all profiles (Argo float
22 and shipboard CTD profiles) were taken coincidentally inside of an eddy. This proportion is
23 in the range of earlier results derived by Chaigneau et al. (2011), who estimated that ~23% of
24 their Argo float profiles in the eastern upwelling regions of the Pacific Ocean are conducted
25 in eddies and Pegliasco et al. (2015), who found 38% of all their Argo floats profiles in the
26 eastern upwelling areas conducted in eddies. We could also confirm the result of Pegliasco et
27 al. (2015) that the majority of all Argo float profile in eddies are conducted in long-lived
28 anticyclones/ACMEs.

29 However, we are interested in the anomalous water mass characteristic inside the eddy
30 compared to the surrounding water. Anomaly profiles of potential temperature, θ , salinity, S,
31 and potential density, σ_θ , were derived as the difference of the profiles inside and reference
32 profiles outside of an eddy. Profiles outside of eddies are required to be taken within a
33 maximum distance of 120 km from the eddy center and at maximum ± 25 days apart from the
34 time the profile inside of the eddy was taken (Figure 4). For 176 profiles out of the 1174

1 profiles inside of eddies no reference profile could be found fulfilling these criteria. In total
2 587 anomaly profiles for anticyclones/ACMEs and 411 anomaly profiles for cyclones were
3 derived. As mentioned before it was useful to further separate anticyclonically rotating eddies
4 into two types: conventional anticyclones with downward bending isopycnals (and isotherms)
5 throughout and ACMEs with upward bending isopycnals in the upper 50 to 100 m depth and
6 downward bending isopycnals below. As a consequence, the MLD inside the ACMEs is
7 shallower compared to background values, while it can be several tens of meters deeper in
8 conventional anticyclones. We used the MLD difference to proof the separation into
9 conventional anticyclones and ACMEs from the satellite based surface signatures, described
10 above. In all cases, where the MLD inside of an anticyclonically rotating eddy was at least
11 10 m shallower than the MLD outside the eddy, the eddy was associated with a negative SST
12 anomaly. Hence, the eddy type separation through satellite based surface signatures appears to
13 be accurate. The separation identified 95 out of 587 profiles in anticyclonically rotating eddies
14 as being taken in ACMEs (Figure 5). Averaging all anomaly profiles for anticyclones,
15 cyclones and ACMEs yields mean anomaly profiles for potential temperature, $\bar{\theta}'$, salinity, \bar{S}' ,
16 and potential density, $\bar{\sigma}_{\theta}'$, for the three different eddy types. Profiles of available heat and salt
17 anomalies (AHA [J m^{-1}] and ASA [kg m^{-1}]) per meter on the vertical were then derived as:
18

$$AHA = \pi r^2 \rho C_p \bar{\theta}', \quad (1)$$

$$ASA = 0.001 \cdot \pi r^2 \rho \bar{S}', \quad (2)$$

19
20 where ρ is density (in kg m^{-3}), C_p is specific heat capacity ($4186.8 \text{ J kg}^{-1} \text{ K}^{-1}$), and r is the
21 mean radius. The factor 0.001 in (2) is an approximation to convert PSS-78 salinity to salinity
22 fractions (kg of salt per kg of seawater). These calculations are partly adapted from
23 Chaigneau et al. (2011), where AHA and ASA are computed for eddies in the East Pacific.
24 Integrating AHA and ASA per meter over the depth range 0 to 350 m, the AHA_{total} (in J) and
25 ASA_{total} (in kg) was obtained. The lower boundary of integration was chosen as below 350 m
26 no significant temperature and salinity anomalies could be identified for the composite eddies
27 of the three eddy types.

28 Eddies that pinch off from the eastern boundary are expected to carry waters with SACW
29 signature westward into areas where waters with NACW signature prevail. To quantify the
30 amount of SACW carried by these eddies, we follow a method developed by Johns et al.
31 (2003) used to quantify the amount of water of southern hemisphere origin carried by North
32 Brazil Current rings. Accordingly the highest/lowest 10% of the salinity values on potential

1 density surfaces were averaged to define the mean NACW/SACW characteristics in the
2 region as function of potential density. The obtained characteristics were used to determine
3 the percentage of SACW contained in any profile taken inside and outside of eddies.
4 Anomaly profiles of SACW percentage as function of potential density were then calculated
5 as the difference of the profiles inside and outside of eddies and were eventually transformed
6 back into depth space using a mean density profile.

7 To illustrate mean anomalies in potential temperature, salinity, potential density and SACW
8 percentage for each eddy type as a function of depth and radial distance, the available profiles
9 were sorted with respect to a normalized distance, which is defined as the actual distance of
10 the profile from the eddy center divided by the radius of the eddy. The profiles were grouped
11 and averaged onto a grid of 0.1 between 0 and 1 of the normalized radial distance. Finally the
12 field was mirrored at zero distance and a running mean over three consecutive horizontal grid
13 points was applied.

14 **2.4 Determining the heat, salt and volume transport**

15 The three-dimensional structures of composite cyclones, anticyclones and ACMEs produced
16 out of the combination of altimetry data and all available profiles were used to estimate the
17 relative eddy contribution to fluxes of heat, salt and volume in the TANWA. Here we chose to
18 define enclosed areas with Area I representing the extended boundary current region, Area II
19 the transition zone and Area III the subtropical gyre region. By multiplying the heat transport
20 of the composite eddies with the amount of eddies dissolving during a year in a given area
21 (corresponding to an flux divergence) a mean heat release (in $W m^{-2}$) and a mean salt release
22 (in $kg m^{-2}$) was calculated. The mean heat release can be compared to the net atmospheric
23 heat flux in the area here derived from the NOC Surface Flux Dataset (Berry and Kent, 2011).
24 Using the volume of a composite eddy (defined by the mean radius and the depth range 0 to
25 350 m) and the mean SACW percentage within the eddy, the total volume transport of SACW
26 of cyclones, anticyclones and ACMEs was calculated.

27

1 **3. Results and Discussion**

2 **3.1 Eddy statistics from SLA data**

3 The two eddy tracking methods applied to the SLA data detected ~2800 eddies over the 19
4 years of analysed data (Table 2, Figure 6) with slightly more cyclones than
5 anticyclones/ACMEs (6% more in the OW-method, 2% more in the GEO-method). Note, that
6 the given number of eddies must be seen as lower limit due to the coarse resolution of the
7 satellite products. All of the detected eddies are nonlinear by the metric U/c , where U is the
8 maximum circumpolar geostrophic surface velocity and c is the translation speed of the eddy.
9 A value of $U/c > 1$ implies that fluid is trapped within the eddy interior (Chelton et al., 2011)
10 and exchange with the surrounding waters is reduced. Many of the eddies are even highly
11 nonlinear, with 60% having $U/c > 5$ and 4% having $U/c > 10$.

12 Considering only the period after 1998, i.e. when our SST data set becomes available, a
13 satellite data-based separation between anticyclones (positive SST anomalies) and ACMEs
14 (negative SST anomalies) is possible. We found that about 20% of the anticyclonically
15 rotating eddies are ACMEs. However, the number of ACMEs might be underestimated,
16 because ACMEs are associated with a weak SLA signature and therefore more difficult to
17 detect with the SLA-based algorithms. Also the nonlinearity of ACMEs is underestimated by
18 using geostrophic surface velocity as they have a subsurface velocity maximum.

19 Although the GEO-method in general detects slightly more eddies than the OW-method (in
20 total 75 eddies more, which is 2.7% more than the OW-method) the situation is different near
21 the coastal area where the OW-method detects 30 eddies per year but the GEO-method only
22 22 eddies per year. This results from the strong meandering of the boundary current, where
23 meanders are sometimes interpreted as eddies by the OW-method due to the high relative
24 vorticity. In contrast, the GEO-method uses closed streamlines and therefore does not detect
25 meanders as eddies, which makes this method more suitable for eddy detection in coastal
26 areas. The average eddy radius in the TANWA is found to be 56 ± 12 km (given here as mean
27 and standard derivation) with the GEO-method resulting in around 10 km larger radii but also
28 with a four times higher standard deviation when compared with the OW-method. The
29 difference in the standard deviation of the eddy radius derived from GEO and the OW-method
30 is partly due to the identification of few very large eddies using the GEO-method, which is
31 not the case for the OW-method. In general, the OW-method appears to be the more reliable
32 tool for identifying the eddy surface area and the corresponding radius in the TANWA.

33 Both algorithms show that on average the anticyclones and ACMEs are larger and have a

1 longer lifetime than the cyclones. The average westward propagation speed is 3.00 ± 2.5 km
2 d^{-1} for all eddy types, which is on the order of the first baroclinic mode Rossby wave phase
3 speed at that latitude range (Chelton et al., 1998). The average tracking period (or lifetime) of
4 an eddy in the TANWA is 28 days with a high standard deviation of 28 days. The longest
5 consecutive tracking period for a single eddy (found similar in both algorithms) was around
6 280 days for an anticyclone, 180 days for a cyclone and 200 days for an ACME. However,
7 most of the eddies were detectable for a period of 7 to 30 days. The number of eddies
8 decreases rapidly with increasing tracking period (Figure 6). Note that the OW-method
9 detects 450 eddies with a lifetime between 7-14 days, which is more than the GEO-method.
10 However, for longer lifetimes the GEO-method detects more eddies than the OW-method. As
11 the tracking procedure in both algorithms is the same, the GEO-method seems to be more
12 reliable in identifying and following eddy like structures from one time step to another. The
13 percentage of tracked anticyclones/ACMEs and cyclones is close to 50% for short tracking
14 periods. For longer lifetimes anticyclonic eddies tend to dominate, this is also reflected in the
15 slightly shorter mean lifetimes of cyclones compared to anticyclones. The dominance of long-
16 lived anticyclones is also shown in the observational studies of Chaigneau et al. (2009),
17 Chelton et al. (2011) and theoretically suggested by Cushman-Roisin and Tang (1990). The
18 latter authors showed that in an eddy environment anticyclonic eddies are generally more
19 robust and merge more freely than cyclones producing long-lived eddies, while cyclones
20 show a higher tendency to self-destruction.

21 Note, that tracking of eddies in the TANWA is prone to errors in particular regarding the
22 information about the eddies' lifetime. Some eddies disappear in single SLA maps, which is
23 at least partly due to the separation of the satellite ground tracks (Chaigneau et al., 2008). In
24 order to avoid losing an eddy, we search two weeks after its assumed disappearance within a
25 defined radius for an eddy with the same polarity (see section 2.1.2). The fact that purest
26 SACW, which in the TANWA occurs in the eastern boundary region, is found regularly in
27 eddy cores at the CVOO mooring (~850 km offshore) (Karstensen et al., 2015) shows that
28 long-lived eddies must exist in the TANWA. Hence, the eddy tracking algorithms
29 underestimate the eddy lifetime and accordingly overestimate the amount of newly generated
30 eddies.

31 This challenge for the eddy tracking algorithms in the TANWA is probably the reason why
32 Chelton et al. (2011) and Chaigneau et al. (2009) could not detect many long-lived eddies in
33 this area. Their definition of long-lived eddies requires eddies to be trackable for longer than
34 112 days (Chelton et al., 2011) or 35 days (Chaigneau et al., 2009). With the adaption of the

1 method for the TANWA with the two weeks search radius as described above, eddy tracking
2 has improved, however some eddies might still be lost. In addition, the mean eddy lifetime of
3 eddies in TANWA is underestimated due to the restriction of eddy trajectories at the northern,
4 southern and western boundaries.
5

6 **3.2 Generation areas and pathways**

7 To identify hot spots of eddy generation, the locations of the first detection of each eddy is
8 counted in $1^\circ \times 1^\circ$ boxes (Figure. 7). The OW-method and the GEO-method do not show a
9 significantly different pattern, except near the coast, where the local maximum in the number
10 of newly detected eddies is shifted slightly offshore for the GEO-method compared to the
11 OW-method. However, the distribution shows that most eddies are generated in the coastal
12 area along the shelf. Within this region the headlands of the coast seem to play an important
13 role as about 9 newly detected eddies per year are found around Cap Vert (Senegal), about 4
14 eddies per year off Saint-Louis (Senegal) and about 5 eddies per year off Cap Timris
15 (Mauretania). At these spots the algorithms detect more than 70% of the newly detected
16 eddies (18 out of 25) per year in the coastal area. Another location of high eddy generation is
17 southeast of the Cape Verde Islands, especially south of the northwesternmost Island Santo
18 Antão with about 2 newly detected eddies per year and southwest of Fogo with about 5 newly
19 detected eddies per year.

20 To identify the preferred eddy propagation pathways, the locations of eddy centers, which
21 were tracked for longer than one month (35 days), were counted in $1/6^\circ \times 1/6^\circ$ boxes over all
22 time steps. The spatial distribution of eddy activity indeed shows some structures and eddies
23 tend to move along distinct corridors westward, away from the coast into the open ocean
24 (Figure 8) as also shown for the Canary Island region (Sangrà et al., 2009). The propagation
25 pathways can be separately investigated for the different eddy types: Most of the anticyclones
26 are generated along the coast south of Cap Timris, off Saint-Louis and north off Cap Vert.
27 They propagate either north of 18°N from their generation areas westward into the open
28 ocean or south of 18°N with a southward deflection offshore. Their mean westward
29 propagation speed is $3.05 \pm 2.15 \text{ km d}^{-1}$. Other generation hotspots for anticyclones are
30 around the Cape Verde Islands south of Santo Antão and south of Fogo. For cyclones the
31 generation areas are more concentrated than for anticyclones. North of Cap Timris and off
32 Cap Vert are the main hotspots near the coast. On their way westwards cyclones tend to have
33 a northward deflection in their pathways. The hotspot for cyclone generation around the Cape
34 Verde islands is west of Fogo. Cyclones have a mean westward propagation speed of $2.9 \pm$

1 2.15 km d⁻¹. Although not significantly different, the larger westward propagation speed of
2 anticyclones compared to cyclones does agree with theoretical considerations regarding the
3 westward eddy drift on a beta-plane (Cushman-Roisin et al., 1990).

4 The main generation areas for ACMEs near the coast are north of Cap Timris and off Saint-
5 Louis around 18°N. ACMEs generated north of Cap Timris tend to have a slightly southward
6 deflection on their way westwards into the open ocean, whereas the eddies generated off
7 Saint-Louis show no meridional deflection and propagate along ~18°N into the open ocean.
8 Their mean westward propagation speed is 3.05 ± 2.1 km d⁻¹. The main generation area of
9 ACMEs near Cape Verde Islands is located south of the northwesternmost island Santo
10 Antão.

11

12 **3.3 Seasonal variability of eddy generation**

13 While the two eddy detection methods differ mostly in the number of identified eddies close
14 to the coast, the season of peak eddy generation is very stable for both methods. A
15 pronounced seasonality with a maximum of newly formed eddies during boreal summer
16 (June/July), is obtained from both methods (Figure 9). During April to June newly generated
17 eddies are mostly cyclonic, while during October to December newly generated eddies are
18 mostly anticyclonic (anticyclones plus ACMEs). These seasonal differences indicate different
19 eddy generation mechanisms at play in the TANWA during the different seasons. Different
20 mechanisms for the generation of eddies in eastern boundary upwelling regions have been
21 proposed (e.g. Liang et al. (2012)). Barotropic and baroclinic instabilities of the near coastal
22 currents (Pantoja et al., 2012) triggered by e.g. the passage of poleward propagating coastal
23 trapped waves (Zamudio et al. (2001), Zamudio et al. (2007)), wind perturbations (Pares-
24 Sierra et al., 1993) or interactions of the large-scale circulation with the bottom topography
25 (Kurian et al., 2011) are the main processes identified for the eddy generation in eastern
26 boundary upwelling regions. In the TANWA, the period of maximum eddy generation
27 (June/July) is characterized by a strong near-surface boundary current, the MC (Lázaro et al.,
28 2005) suggesting dynamic instabilities of the boundary current as an important generation
29 mechanism. However, there is a difference in peak generation of cyclones and anticyclones.
30 While the maximum generation of cyclones occurs in June during the acceleration phase of
31 the MC, the seasonality of anticyclone generation is not as distinct with weaker maxima in
32 July and at the end of the year. The generation of ACMEs has the main peak in April to May,
33 which is at the end of the upwelling season. During that period the PUC is likely getting
34 unstable and vanishes later on (Barton, 1989).

1 The seasonal peak in eddy occurrence appears to propagate westwards into the open ocean.
2 To illustrate this, annual harmonics are fitted to the number of eddies detected per month in 2°
3 $\times 2^\circ$ boxes (Figure 10). Note, that the phase of a box is only shown when the amplitude is
4 larger than 2.5 eddies per box. After the main generation of cyclones in the coastal area in
5 June, the eddies enter the open ocean in late boreal autumn, passing the Cape Verde Islands
6 and the ventilated gyre regime north of the CVFZ in boreal winter/spring. As mentioned
7 before anticyclones are generated one to a few months later at the coast (July and October,
8 November). They dominantly reach the open ocean in boreal winter and spring and
9 accordingly pass the Cape Verde Islands and the ventilated gyre regime north of the CVFZ in
10 late boreal spring and summer. Note, that the relatively clear signal of the annual harmonic of
11 eddy detections (Figure 10) also suggests that eddies with lifetime > 9 months are more
12 frequent in the TANWA than indicated by the statistical output of the algorithms.

13 **3.4 Mean eddy structure**

14 **3.4.1 Surface anomalies related to eddies**

15 For the three types of eddies, composite were constructed from daily SLA, SST, and SSS
16 anomaly fields. An area of 300 km \times 300 km around every identified eddy center (center =
17 maximum value of SLA) was considered (Figure 11). Overall we had about 40.000 snapshots
18 of eddies between 1993 and 2013 available to calculate the mean SLA and SST anomalies. To
19 derive mean SSS anomalies, only about 10.000 snapshots were merged because of the shorter
20 time period of the SSS satellite data record (2010-2013).

21 For anticyclones, we found a positive SLA (maximum value in the eddy core is 6.9 cm
22 (3.02 cm; 11.01 cm), given here as mean and the upper and lower limits of the 68% quartile
23 range), a positive SST anomaly (maximum value in the eddy core 0.13 $^\circ\text{C}$ (0.03 $^\circ\text{C}$; 0.24 $^\circ\text{C}$))
24 and a positive SSS anomaly (maximum value in the eddy core is 0.20 (-0.04; 0.52)). For
25 cyclones, we found a negative SLA (minimum value in core -5.5 cm (-1.57 cm; -7.37 cm), a
26 negative SST anomaly (minimum value in the core is -0.15 $^\circ\text{C}$ (-0.04 $^\circ\text{C}$; -0.30 $^\circ\text{C}$)) and a
27 negative SSS anomaly (minimum value in the core is -0.16 (0.08; -0.48)). However, for the
28 ACMEs (about 20% of the anticyclones) we found a negative SST anomaly (minimum value
29 in the core is -0.15 $^\circ\text{C}$ (-0.04 $^\circ\text{C}$; -0.31 $^\circ\text{C}$) was observed. The vertical structure of these
30 anticyclones as obtained from temperature and salinity profiles revealed the characteristic
31 pattern of ACMEs with a very shallow mode in the upper 100 m or so. ACMEs also have a
32 negative SSS anomaly (minimum value in the core is -0.13 (0.10; -0.33)). For all eddy types,
33 SST dominates sea surface density.

34 Compared to SLA and SST measurements, the satellite-based observations of SSS are

1 afflicted with high uncertainties and large measuring gaps. However, in the composite it is
2 possible to detect eddy type dependent anomalies, even if they are not as clear and circular
3 than the SLA and SST anomalies. The zonally stretched structures in the composites of SSS
4 anomalies may also result from the coarser temporal resolution of SSS data (i.e. 10 days)
5 resulting in a smearing of the eddy signal in the direction of propagation. Note, that the
6 composites of SSS anomalies showed only coherent eddy structures when selecting energetic
7 eddies (i.e., with a radius between 45-70 km and an absolute SLA anomaly >2 cm). The
8 composites of SLA and SST anomalies are much less affected by the restriction with regard to
9 the eddy amplitude.

10

11 In summary, the absolute SST and SSS anomalies of all three eddy types are of similar
12 magnitude. The magnitude of absolute SLA of anticyclones and cyclones is also somehow
13 similar, while ACMEs have a weaker SLA signature (which makes them more difficult to be
14 detected and tracked by satellite altimetry). The maximum surface circumpolar velocity is
15 0.18 ± 0.12 m s⁻¹ in cyclones, 0.17 ± 0.12 m s⁻¹ in anticyclones and 0.16 ± 0.10 m s⁻¹ in
16 ACMEs. Overall, cyclones are slightly smaller, rotate faster and therefore have a shorter
17 lifetime than the other eddy types.

18

19 **3.4.2 Vertical structure of eddies**

20 Profiles from Argo floats, shipboard CTD and moorings were used to derive a mean vertical
21 eddy structure. Here, we calculated anomaly profiles of potential temperature, salinity and
22 potential density derived from profiles inside and outside of eddies. The mean vertical
23 structure and the anomalies presented here (Figure 12) are based on 492 profiles in
24 anticyclones, 411 profiles in cyclones but only 95 profiles in ACMEs. Consequently, the
25 statistics for ACMEs are weakest and the mean vertical structure must be interpreted with
26 care. Cyclones, anticyclones and ACMEs are characterised by a different
27 shallowing/deepening of isopycnal surfaces. Anticyclones carry a warm and saline water
28 anomaly, whereas cyclones and ACMEs host cold and less saline water in their cores. The
29 effect of temperature anomalies on density anomalies dominates over the effect of salinity
30 anomalies, which results in a positive density anomaly associated with cyclones (shoaling of
31 isopycnals) and a negative density anomaly associated with anticyclones (deepening of
32 isopycnals). This is illustrated by the elevation (deepening) of 25 m (36 m) of the density
33 surface of 26.2 kg m⁻³ in the core of the cyclone (anticyclone) compared to the surroundings.

1 Due to the specific vertical structure of ACMEs, characterized by a strengthening of the
2 anticyclonic rotation with depth in its upper part and a weakening of the anticyclonic rotation
3 in its lower part, the ACMEs have a positive density anomaly in about the upper 100 m
4 (shoaling of isopycnals) and a negative density anomaly below down to about 350 m
5 (deepening of isopycnals). The mode-water in the core of the ACMEs is only weakly
6 stratified. This is illustrated by the elevation of 48 m of the density surface of 26.2 kg m^{-3}
7 slightly above the core and the deepening of 52 m of the density surface of 26.7 kg m^{-3} below
8 the core compared to the surroundings. From the mean vertical eddy profiles, we diagnose a
9 maximum temperature anomaly underneath the mean mixed layer depth, which is at depth of
10 about 50m. It is $-2.42 \pm 1.23 \text{ }^\circ\text{C}$ at 55 m for cyclones and $+1.88 \pm 1.37 \text{ }^\circ\text{C}$ at 54 m for
11 anticyclones. The maximum salinity anomaly is -0.34 ± 0.25 at 70 m depth for cyclones and
12 $+0.25 \pm 0.2$ at 100 m for anticyclones and as such located below the maximum temperature
13 anomaly. The respective maximum density anomalies are, as expected, close to the location of
14 the maximum temperature anomaly, and are $0.28 \pm 0.42 \text{ kg m}^{-3}$ at 48 m for cyclones and 0.44
15 $\pm 0.35 \text{ kg m}^{-3}$ at 50 m for anticyclones. The mean ACME structure is characterized by a much
16 stronger temperature anomaly of $-4.0 \pm 2.2 \text{ }^\circ\text{C}$ at 51 m depth and salinity anomaly of $0.72 \pm$
17 0.38 at 74 m depth in comparison to cyclones and anticyclones. Note, that the cold and fresh
18 SACW in the ACME core does not produce a positive temperature anomaly when it reaches
19 deeper levels due to the downward bending of isopycnal surfaces below the eddy core. The
20 ACME density anomaly has a maximum of $0.66 \pm 0.35 \text{ kg m}^{-3}$ at about 47 m and a minimum
21 of $-0.08 \pm 0.06 \text{ kg m}^{-3}$ at about 168 m, which reflects the shoaling and deepening of
22 isopycnals towards the eddy center above and below its core. Note, that below the eddy core
23 (>150 m depth) horizontal density anomalies are dominated by salinity with temperature
24 playing a minor role. For all eddy types, cyclones, anticyclones and ACMEs, temperature,
25 salinity and density anomalies reach down to about 300-350 m depths with a maximum
26 beneath the mixed layer or slightly deeper.

27 Chaigneau et al. (2011) observed mean maximum anomalies of $\pm 0.7 \text{ }^\circ\text{C}$ in temperature and \pm
28 0.06 in salinity based on Argo float measurements in eddy cores within the Southeast Pacific.
29 For the TANWA the mean maximum anomalies of about $\pm 2 \text{ }^\circ\text{C}$ in temperature and ± 0.3 in
30 salinity are more than twice as high. The presence of different water masses, cold and fresh
31 SACW prevailing in the coastal region and warmer and saltier NACW further offshore,
32 results in the large temperature and salinity anomalies in eddy cores in the TANWA
33 compared to the Southeast Pacific. Furthermore the reference used for calculating an anomaly
34 can create large differences. Chaigneau et al. (2011) computed the anomalies of Argo float

1 profiles relative to interpolated climatological profiles taken from CSIRO Atlas of Regional
2 Seas (CARS). Here, we tested five different references to calculate anomalies and found
3 significantly different anomalies, even with reversed sign (Table 3). The differences in the
4 mean anomalies depend on the used reference profiles. Besides the “next profile outside”, we
5 used different climatologies as reference. However, differences in temperature and salinity
6 between the different climatologies are of similar magnitude than the derived mean anomalies
7 of the different eddy types (Table 1). When using the “next profile outside” as reference we
8 obtained larger mean anomalies, which could suggest that the “next profile outside” is
9 systematically biased by nearby eddies of reversed polarity (which are possibly not well
10 identified by the eddy detecting methods). However, in particular in regions with strong
11 gradients/fronts (e.g., CVFZ, coastal upwelling) with strong seasonality and variability, the
12 “next profile outside” should deliver the most realistic background condition surrounding an
13 eddy and thus should be preferably used to calculate water mass anomalies transported by
14 eddies.

15 Here, we want to note that the uppermost data point (at 5 m) of the mean temperature and
16 salinity anomaly profiles of the three types of eddies from the selected in-situ data (Figure 12)
17 agrees well with the surface anomalies based on satellite data composites (Figure 11) and
18 amounts to maximum values of $-0.15\text{ }^{\circ}\text{C}$ (in-situ: $-0.15\text{ }^{\circ}\text{C}$) for cyclones, $0.13\text{ }^{\circ}\text{C}$ (in-situ:
19 $0.25\text{ }^{\circ}\text{C}$) for anticyclones and $-0.15\text{ }^{\circ}\text{C}$ (in-situ: $-0.20\text{ }^{\circ}\text{C}$) for ACMEs; corresponding salinity
20 anomalies are -0.16 (in-situ: -0.10) for cyclones, 0.2 (in-situ: 0.13) for anticyclones and -0.13
21 (in-situ: -0.11) for ACMEs.

22

23 **3.5 Contribution of eddies to zonal transport of properties**

24 **3.5.1 Thermohaline content and associated transport of eddies**

25 For all cyclones/anticyclones/ACMEs a mean eddy volume of $2.860 \times 10^{12}\text{ m}^3 / 3.089 \times 10^{12}\text{ m}^3$
26 $/ 2.973 \times 10^{12}\text{ m}^3$ is derived, considering their mean radii (51 km/53 km/52 km) and a mean
27 depth of 350 m for all three eddy types. Distributed over a period of one year this leads to a
28 westward volume flux associated with a single eddy of about 0.1 Sv.

29 The mean three-dimensional structure of temperature and salinity anomalies associated with
30 cyclones, anticyclones and ACMEs (Figure 12) was used to estimate profiles of AHA and
31 ASA per meter (Figure 13). The maximum AHA per meter is located at depths comparable to
32 the maximum temperature anomaly and at about 55 m for all eddy types. The maximum ASA
33 per meter is located deeper at about 80 m depth (~ 70 m depth for cyclones, ~ 80 m for ACMEs
34 and ~ 110 m for anticyclones). The $\text{AHA}_{\text{total}}$ ($\text{ASA}_{\text{total}}$), derived by integrating the profiles of

1 AHA (ASA) per meter from the surface to 350 m, is -14.5×10^{18} J (-73.0×10^{10} kg) for
2 cyclones, 11.0×10^{18} J (40.7×10^{10} kg) for anticyclones and -15.4×10^{18} J (-94.2×10^{10} kg)
3 for ACMEs (see also Table 4).

4 Comparing our results to the Southeast Pacific (cyclones: $AHA_{total} = -5.5 \times 10^{18}$ J,
5 $ASA_{total} = -9.8 \times 10^{10}$ kg; anticyclones: $AHA_{total} = 8.7 \times 10^{18}$ J, $ASA_{total} = 23.8 \times 10^{10}$ kg)
6 (Chaigneau et al., 2011), we found an overall smaller volume of the eddies in the TANWA,
7 but derived larger heat and salt anomalies. On the one hand this could be explained by the fact
8 that we average over a smaller area. However, regional differences should also exist e.g.
9 related to the boundary current hydrographic structure or the mean rotation speed (hence
10 bending of isopycnals). For ACMEs in the Southeast Pacific there is only one recent estimate
11 by Stramma et al. (2013) for comparison, who estimated the AHA_{total} and ASA_{total} of a well-
12 observed ACME to be 17.7×10^{18} J and 36.5×10^{10} kg, respectively. The heat and salt
13 anomalies are of the same order as found for the mean ACME in the TANWA but with
14 reversed sign, which is remarkable. The ACME observed in the Southeast Pacific transports
15 in contrast to the composite ACMEs in the TANWA warm and saline waters in its core
16 offshore. One possible explanation is the different water mass characteristics in the source
17 (coastal) region of the ACMEs in the Southeast Pacific compared to the TANWA.

18 Evenly distributed over a period of one year the heat (salt) transport associated with one
19 single eddy is -4.6×10^{11} W (-23.2×10^3 kg s^{-1}) for cyclones, 3.5×10^{11} W (12.9×10^3 kg s^{-1})
20 for anticyclones, and -4.9×10^{11} W (-29.9×10^3 kg s^{-1}) for ACMEs. As expected from the
21 lower AHA_{total} (ASA_{total}) that has been derived for eddies in the Southeast Pacific (Chaigneau
22 et al., 2011), the heat (salt) transport due to eddies in the TANWA is comparably large (see
23 also Table 4).

24 In order to estimate the large-scale impact of the heat and salt transport by these eddies in the
25 TANWA, we define three characteristic areas (see Figure 14): the extended boundary current
26 region (Area I), the transition zone (Area II), and the subtropical gyre region (Area III). Based
27 on the results from the GEO-method, 21 eddies are formed each year in the extended
28 boundary current region of the TANWA. While about 5 eddies dissipate quickly and only
29 influence the near coastal regions, about 16 eddies per year leave the extended boundary
30 current region and propagate into the transition zone of the TANWA (Figure 14a). Based on
31 the mean temperature and salinity anomalies derived above, it equates to a heat (salt)
32 transport of -35.9×10^{11} W (-180.6×10^3 kg s^{-1}) by cyclones, 23.0×10^{11} W (85.3×10^3 kg s^{-1})
33 by anticyclones and -8.8×10^{11} W (-53.8×10^3 kg s^{-1}) by ACMEs. With regard to the number
34 of eddies that dissolve in the different areas per year an “equivalent surface heat flux” (ESHF)

1 is computed and compared with the annual mean net surface heat flux for the respective
2 regions as taken from the NOC Surface Flux Dataset (Berry and Kent, 2011) (Figure 14b).
3 The anomalies in heat and salt associated with the three different types of eddies partly
4 counteract each other. Anomalies in cyclones and ACMEs are negative, indicating heat and
5 salt deficiencies in their core, while anomalies in anticyclones represent a surplus of heat and
6 salt with respect to the background conditions. The cyclonic eddies provide an ESHF in Area
7 II of about -3.0 W m^{-2} , anticyclones of about $+2.0 \text{ W m}^{-2}$, and ACMEs of about -0.6 W m^{-2} ,
8 which results in a net ESHF associated with all eddies of about -1.6 W m^{-2} . This heat flux due
9 to eddies represents about 10% of the net surface heat flux in the transition zone of the
10 TANWA that is about $+17.4 \text{ W m}^{-2}$.
11 In the open ocean of the TANWA, cyclones and ACMEs contribute to a cooling and
12 freshening of the upper ocean and anticyclones to a warming and salinity increase. As such,
13 the mesoscale eddy field and its seasonal to interannual variability can have an impact on the
14 regional heat and salt budgets of the TANWA. However, because our calculations only
15 account for long-lived eddies with a radius larger than 45 km, the calculated absolute eddy
16 fluxes represent a lower limit that might increase when accounting also for short-lived, non-
17 coherent eddies and/or sub-mesoscale variability.

18

19 **3.5.2 Zonal eddy dependent westward transport of SACW**

20 Many of the eddies that originate in the eastern boundary region carry water of South Atlantic
21 origin westward. In order to quantify the SACW signature in the eddies, a water mass analysis
22 was performed. For all isopycnals SACW (labelled 100%) and NACW (labelled 0%)
23 temperature and salinity pairs were defined using extremes of all observational data (see
24 Figure 2). Then the percentages of SACW concentrations contained inside the eddy cores
25 were estimated. However, because the background field also transitions along the eddy
26 trajectories towards stronger NACW characteristic, we estimated the SACW content of the
27 eddies relative to the surrounding waters. Figure 15 shows the average vertical structure of the
28 trapped SACW anomaly relative to the background for each eddy type. The different eddy
29 types have a different potential in trapping SACW in their cores. Cyclones contain on average
30 16% (maximum core value: 35%) more SACW than the surrounding water and ACMEs even
31 21% (maximum core value: 60%). This implies a negative heat and salt anomaly along
32 isopycnal layers inside of cyclones and ACMEs. Furthermore it shows the prominent
33 capability of ACMEs to trap and isolate anomalous water inside their cores. In contrast, the
34 SACW anomaly in anticyclones is weak and negative (on average -4% ; minimum core value -

1 10%), implying that anticyclones contain on average a positive heat and salt anomaly along
2 isopycnal layers. As such, anticyclones counteract the westward transport of SACW
3 associated with the propagation of cyclones and ACMEs. Anticyclones instead transport small
4 amounts of NACW westward.

5 To estimate an absolute transport of SACW from the eddy generation area at the eastern
6 boundary into the open ocean, the mean percentages of SACW contained inside the different
7 eddy types can be used. Highest percentage of SACW (>80%) is found in the extended
8 boundary current region (Area I). Northwestward towards the open ocean the SACW
9 percentage decreases (Area II ~ 57%, Area III < 23%; Figure 16b). Hence, when the eddies
10 are generated in the extended boundary current region (in Area I) they trap waters with
11 SACW signature in their cores and transport it westward into the open ocean (Area II and
12 Area III), where waters with NACW signature prevail. These anomalous properties with
13 respect to the surrounding waters can be visualized in a salinity versus sigma-theta diagram
14 (Figure 16a). ACMEs exhibit the strongest SACW signature, indicating again that ACMEs
15 have the best capability to trap water. The percentage of SACW in the different eddy types
16 within the three separated areas are shown in the white circles in Figure 16b. Again the strong
17 capability of ACMEs to transport SACW is obvious. In Area II (background ~57% SACW)
18 ACMEs still exhibit 82% SACW and in Area III (background <23% SACW) it is 78%
19 SACW, indicating that ACMEs are only weakly affected by lateral and vertical mixing.
20 Cyclones contain 69% SACW in Area II and 52% SACW in Area III and as such lose SACW
21 signature from their cores much faster. Anticyclones with 59% SACW in Area II and 29%
22 SACW seem to have almost the same SACW signature as the background. This indicates that
23 either they are not well isolated, and their cores are already replaced with the surrounding
24 water, or that they are transporting low SACW signatures in their cores from the beginning.

25 Using the number of eddies passing the boundaries of the areas and the “excess” percentage
26 of SACW in their cores (relative to the background), an “eddy type dependent” absolute
27 transport of SACW out of the boundary current was derived (Figure 16b). We obtained an
28 absolute transport of 2.07 Sv of SACW out of the boundary current near the coast into the
29 extended boundary current region (Area I) of which about 0.81 Sv of SACW reached the
30 transition zone (Area II). Further to the west, about 0.36 Sv of SACW reached the subtropical
31 gyre region west of the Cape Verde Islands (Area III). Considering the volume of the upper
32 350 m of the transition zone (Area II, $2 \times 10^5 \text{ km}^3$) the eddy transport will replenish the
33 SACW part in about 2.5 years. Note, that these calculations represent conservative
34 assumptions about the SACW transport since the contribution of short-lived, non-coherent

1 and smaller scale eddies to the SACW transport is not included. For example, the highly
2 energetic cyclone generated at the headland of Cap Vert discussed in detail by Alpers et al.
3 (2013), which has a radius of 10 to 20 km and a Rossby number larger than one, is not
4 detected by the eddy detection algorithms used in this paper due to its small scale, but
5 certainly contributed to the westward transport of near-coastal water masses.
6

7 **4. Summary and Conclusion**

8 Within this study we analysed satellite based remotely sensed data, including SLA, SST, SSS,
9 as well as in-situ temperature and salinity profiles, taken from Argo floats, ships and
10 moorings, in order to examine the eddy characteristics and dynamics in the TANWA. Eddies
11 were identified based on their manifestation in SLA data using two different eddy detection
12 algorithms, the OW-method and the GEO-method. Both detection algorithms produced rather
13 similar results except for the open ocean/coastal transition zone, where the OW methods seem
14 to overestimate the amount of eddies due to high vorticity values associated with the
15 meandering boundary current.

16 We found that anticyclones (cyclones) are associated with enhanced (reduced) SLA, enhanced
17 (reduced) SST and enhanced (reduced) SSS in their eddy cores, respectively. However, 20%
18 of all eddies with enhanced SLA showed reduced SST and reduced SSS and we were able to
19 classify these eddies as anticyclonic mode-water eddies (ACMEs). Of the average 146 ± 4
20 eddies detected per year in the TANWA over 19 years of SLA data, the ratio of cyclonic and
21 anticyclonic eddies is nearly equal (52% cyclones, 39% anticyclones, 9% ACMEs), with a
22 similar radius of 56 ± 12 km for all three eddy types.

23 In agreement with earlier findings (Chaigneau et al. (2009)) we found eddies being generated
24 mainly near the coast and here at some topographic “hot spots”. For the TANWA these hot
25 spots are associated with the headlands of Cap Vert (Senegal) and Cap Timris (Mauretania).
26 We could also confirm the existence of a seasonality in the eddy generation (Chaigneau et al.
27 (2009), Kurczyn et al. (2012)) and found cyclones form preferably during April to June, while
28 anticyclones and ACMEs are mostly generated from October to December. After their
29 generation, eddies of all three types propagate westward with a speed, c , of about 3.00 ± 2.15
30 km day^{-1} , which is in general agreement with the first baroclinic mode Rossby wave phase
31 speed at that latitude range (Chelton et al., 1998). We found that anticyclones/cyclones follow
32 distinct corridors with a meridional deflection towards the equator/pole. This is in agreement
33 with the theoretical and observational findings of the deflection from the β -drift of

1 anticyclones and cyclones (Chelton et al., 2011). In contrast, ACMEs do not show a
2 significant meridional deflection.

3
4 We suspect that the eddy generation is related to instabilities of the eastern boundary current.
5 Eddy generation resulting from interactions of coastal currents with headlands is a well-
6 known process and has been extensively investigated (e.g. Røed (1980), Klinger (1994a),
7 Klinger (1994b), Pichevin and Nof (1996), Crawford et al. (2002), Zamudio et al. (2007)).
8 Most likely the generation is driven by flow separation at the headlands of the West African
9 coast, triggered by seasonality in the wind forcing. For the North-Eastern Pacific it has been
10 shown that coastal trapped waves have an impact on the stability of coastal currents and hence
11 eddy generation (Zamudio et al. (2001), Zamudio et al. (2006), Zamudio et al. (2007)). Such
12 eddy generation mechanisms may explain the high eddy generation in the TANWA found
13 during phases of strongest boundary current velocities. However, the detailed investigation of
14 the generation mechanisms of eddies in the TANWA requires realistic high-resolution
15 modelling and is beyond the scope of the present study.

16 The maximum swirl velocity of the eddies, U , as obtained from the surface geostrophic
17 velocity is about $14.7 \pm 9.5 \text{ km day}^{-1}$ indicating a high nonlinearity of the observed eddies, i.e.
18 $U/c > 1$. Due to this nonlinearity the exchange between eddy core and surrounding water is
19 limited and hence they are able to trap water masses and transport them over large distances.
20 In the TANWA the eddies act as transport agents for SACW that is present in the eastern
21 boundary upwelling region toward, and across the CVFZ into the subtropical gyre region,
22 where NACW dominates.

23 In order to estimate the water mass anomalies transported by the different eddy types, their
24 vertical water mass structures were estimated. Cyclones (anticyclones) are associated with
25 maximum temperature/salinity anomalies of about $-2.42 \pm 1.23 \text{ }^\circ\text{C}/ -0.34 \pm 0.25$ ($1.88 \pm$
26 $1.37 \text{ }^\circ\text{C}/ 0.25 \pm 0.2$), respectively, most intense just beneath the mixed layer in the depth
27 range 55 to 100 m. With respect to water mass anomalies the ACMEs stand out because their
28 maximum absolute anomaly is more than twice as large (temperature anomalies of $-4 \pm 2.2 \text{ }^\circ\text{C}$
29 and salinity anomalies of $+0.72 \pm 0.38$) compared to the corresponding anomalies of cyclones
30 or normal anticyclones. Moreover, their mixed layer depth is found at much shallower depth
31 of 40 to 70 m. Given the fundamentally different anomalies that are associated with the two
32 types of eddies with anticyclonic surface flow (normal anticyclones and ACMEs), a separate
33 treatment of these eddy types seems to be mandatory when discussing eddy transports. This
34 has not been done routinely in the past (e.g. Chaigneau et al. (2009), Zhang et al. (2014))

1 primarily because SLA data alone does not provide the necessary information. Here, we were
2 able to distinguish ACMEs from normal anticyclones by using SSS and SST data in parallel.
3 The magnitude of the obtained anomalies varies according to the reference dataset
4 (background data) being used. We tested nearby in-situ data collected outside of eddies as
5 well as different climatological fields (Table 3) as e.g. in Chaigneau et al. (2009). Using the
6 inferred temperature and salinity anomalies we were able to calculate the associated heat
7 (salt) transports for the different eddy types. They amount to -4.6×10^{11} W (-23.15×10^3 kg s⁻¹)
8 for cyclones, 3.5×10^{11} W (12.9×10^3 kg s⁻¹) for anticyclones, and -4.9×10^{11} W ($-29.9 \times$
9 10^3 kg s⁻¹) for ACMEs. Out of the 21 eddies formed each year in the TANWA along the
10 eastern boundary, 5 dissipate in a band of about 250 km width near the coast and about 16
11 propagate into the open ocean adding up to an annual eddy net heat (salt) transport of about
12 50×10^{11} W (-150×10^3 kg s⁻¹). Converting the divergence of the heat transport in the
13 transition zone (Area II) into an equivalent surface heat flux we found a cooling of the ocean
14 of -1.6 W m⁻² due to eddy heat transport, which as such balances about 10% of the net surface
15 heat flux of 17.4 W m⁻² as obtained from the NOC Surface Flux Dataset (Berry and Kent,
16 2011).

17 The TANWA is a crossroad for water masses, with NACW prevailing in the northwest within
18 the ventilated subtropical gyre and SACW in the eastern boundary upwelling region. In order
19 to estimate the dispersal of SACW due to eddies within the TANWA, we analysed the SACW
20 content in the three different eddy types using the in-situ profile data. We found that cyclones
21 contain on average about 16% more SACW than the surrounding water, ACMEs 21%, and
22 normal anticyclones do not carry any SACW anomaly. Some ACMEs efficiently isolate their
23 eddy cores from the surrounding waters reaching maximum SACW anomalies of more than
24 60%, which indicates a high nonlinearity and coherence of these eddies (Karstensen et al.,
25 2015).

26 Considering the total tracer transport of the eddies along isopycnals (spiciness), the negative
27 heat and salt anomaly within cyclones and ACMEs results in a mean water mass transport of
28 2.07 Sv of SACW out of the boundary current region, of which about 0.36 Sv of SACW reach
29 the subtropical gyre region northwest of the Cape Verde Islands. Hence, the SACW transport
30 due to eddies would renew the SACW part of the transition zone located between the
31 extended eastern boundary region and the subtropical gyre region (assuming a layer thickness
32 of 350 m) in about 2.5 years.

33 This study gives a first insight into the types and characteristics of eddies within the TANWA
34 as well as in the fluxes of heat and salt associated with their westward propagation.

1 Remaining open questions regard the importance of short-lived eddies for the transport of
2 heat and salt (which could not be evaluated due to the resolution of the available data sets), as
3 well as the individual processes responsible for eddy generation. The distinction of
4 anticyclonic rotating eddies into ACMEs and “normal anticyclones” seems to be mandatory
5 for future eddy studies as these two eddy types strongly differ in their efficiency to carry
6 water mass anomalies. Moreover, the biogeochemical responses in ACMEs have been found
7 to be very distinct from normal anticyclones and a sufficient representation of both types of
8 anticyclones in coupled physical-biogeochemical models may be crucial for a realistic
9 simulation of eastern boundary upwelling systems.

10 **Acknowledgements**

11 This study is funded by the Deutsche Bundesministerium für Bildung und Forschung (BMBF)
12 as part of the project AWA (01DG12073E) and by the Deutsche Forschungsgemeinschaft as
13 part of the Sonderforschungsbereich 754 “Climate – Biogeochemistry Interactions in the
14 Tropical Oceans” and the project FOR1740 and through several research cruises with RV
15 Meteor, RV Maria S. Merian, RV Poseidon and RV L’Atalante. We thank the captains and
16 crew as well as all chief scientists and scientists of the involved research vessels and our
17 technical group for their help with the fieldwork. Furthermore the authors thank Ping Chang,
18 Rebecca Hummels, Tim Fischer and Robert Kopte for helpful discussions. For ship and
19 mooring data processing we thank Gerd Krahnemann. In addition we thank the international
20 Argo program and the national programs that contribute to it, which collected the data and
21 made it freely available. The Argo program is part of the Global Ocean Observing System.
22 The altimeter products were produced and distributed by *Aviso*
23 (<http://www.aviso.altimetry.fr/>), as part of the Ssalto ground-processing segment. The
24 Microwave OI SST data are produced by Remote Sensing Systems and sponsored by National
25 Oceanographic Partnership Program (NOPP), the NASA Earth Science Physical
26 Oceanography Program, and the NASA MEaSUREs DISCOVER Project. The
27 LOCEAN_v2013 Sea Surface Salinity maps have been produced by LOCEAN/IPSL (UMR
28 CNRS/UPMC/IRD/MNH) laboratory that participates to the Ocean Salinity Expertise
29 Center (CECOS) of Centre Aval de Traitement des Données SMOS (CATDS). This
30 product is distributed by the Ocean Salinity Expertise Center (CECOS) of the CNES-
31 IFREMER Centre Aval de Traitement des Données SMOS (CATDS), at IFREMER,
32 Plouzane (France). The NOCS Surface Flux Dataset v2.0 is distributed from the US National
33 Center for Atmospheric Research (NCAR) and the British Atmospheric Data Centre (BADC).

- 1 The observations used to construct the NOC Surface Flux Dataset come from the
- 2 International Comprehensive Ocean – Atmosphere Data Set (ICOADS).
- 3

1 Tables

2 **Table 1:** Data from the following research cruises were used.

Cruise	Ship	Time	Region	No. of Profiles
Pos 320	Poseidon	March-April 2005	TANWA East	38
M 68/2	Meteor	July 2006	23°W Section	10
M 68/3	Meteor	July-August 2006	18°N Section	81
Pos 347	Poseidon	January-February 2007	TANWA East	125
Pos 348	Poseidon	February 2007	TANWA East	32
Ata 3	L'Atalante	February 2008	TANWA East	58
Ata 4	L'Atalante	March 2008	23°W Section	6
MSM 8	Maria S. Merian	May 2008	South TANWA	3
MSM 10	Maria S. Merian	December 2008	South TANWA	5
Pos 399	Poseidon	May-July 2009	TANWA East	21
M 80/1	Meteor	November 2009	23°W Section	9
M 80/2	Meteor	December 2009	South TANWA	8
M 81/1	Meteor	May 2010	Central TANWA	12
M 83/1	Meteor	December 2010	14.5°N Section	27
MSM 18/2	Maria S. Merian	May 2011	23°W Section	6
MSM 18/3	Maria S. Merian	June 2011	South TANWA	6
MSM 22	Maria S. Merian	November 2012	18°N Section	76
MSM 23	Maria S. Merian	November 2012	14.5°N Section	13
M 96	Meteor	May 2013	14.5°N Section	14
M 97	Meteor	June 2013	14.5°N Section	7
				Σ 557

1 **Table 2:** Mean properties of anticyclones, cyclones and ACMEs in the region of 12°N - 22°N, 16°W– 26°W
2 (TANWA) and their standard deviation given in brackets, detected from the OW-method and the GEO-method
3 (detectable longer than one week and with a radius >45 km). Coastal area is defined as an ~ 250km wide
4 corridor near the coast (see Figure 7). *Note, that the properties of ACMEs are based on less years of SLA data
5 (1998-2013), due to the not available SST data.

Property (based on SLA data between 95-2013)	OW-method			GEO-method		
	Anticyclones	Cyclones	ACMEs*	Anticyclones	Cyclones	ACMEs*
Detected eddies	2741 [144/year]			2816 [148/year]		
	1041 (38%)	1443 (53%)	257 (9%)	1137 (40%)	1422 (51%)	257 (9%)
Detected eddies in coastal area	186 [10/year]	241 [13/year]	43 [2/year]	178 [9/year]	199 [10/year]	45 [3/year]
Average lifetime [days]	30 [±31] max 282	24 [±22] max 176	26 [±28] max 197	32 [±32] max 277	27 [±29] max 180	26 [±28] max 175
Average radius [km]	53 [±5]	51 [±5]	52 [±5]	60 [±20]	62 [±22]	59 [±20]
Average westward propagation [km d ⁻¹]	2.8(±2.4)	2.7(±2.4)	2.8(±2.5)	3.3(±1.8)	3.1(±1.9)	3.3(±1.9)

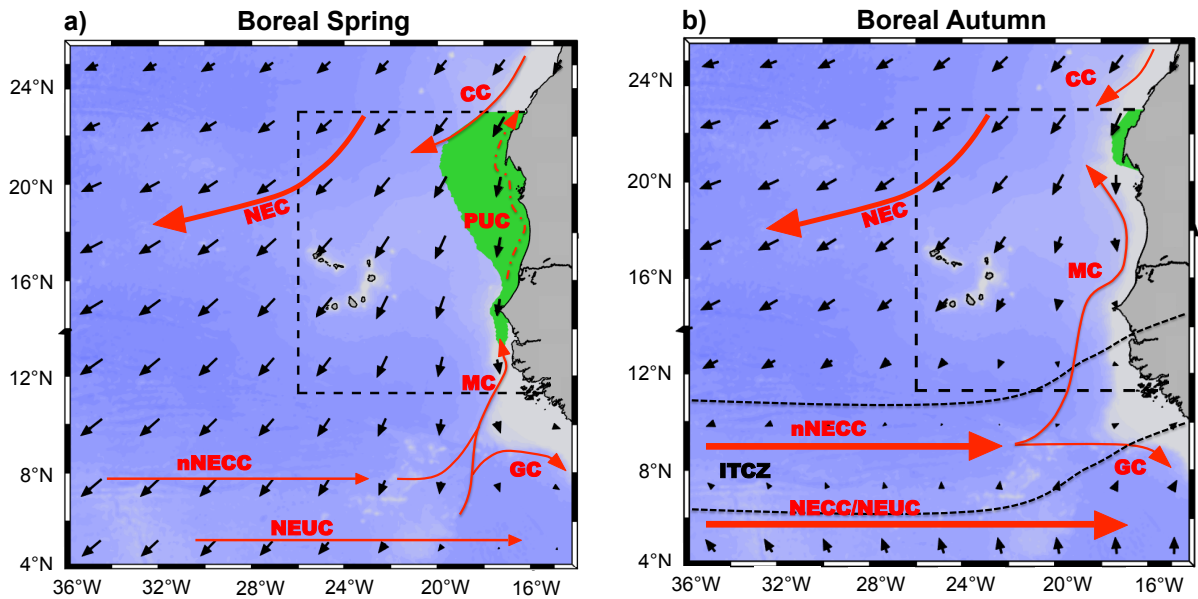
1 **Table 3:** Temperature and salinity anomalies of cyclones and anticyclones vertically averaged in the upper 350
 2 m. Anomaly profiles are calculated relative to different reference datasets: 1.) the nearest in-situ profile in time
 3 and space, 2.) the CSIRO CARS2009a V1.1 climatology, 3.) the monthly WOA09 climatology, 4.) the monthly
 4 MIMOC V2.2 climatology, 5.) the monthly Levitus94 climatology (salt values are not included in monthly
 5 base).

	Cyclones		Anticyclones	
	Temp [°C]	Salt	Temp [°C]	Salt
1.) Next profile outside	-1.22	-0.26	0.87	0.13
2.) CSIRO	-0.21	-0.08	0.94	0.06
3.) WOA	-0.32	-0.10	0.85	0.05
4.) MIMOC	-0.56	-0.32	0.60	-0.17
5.) Levitus	-0.16		0.97	

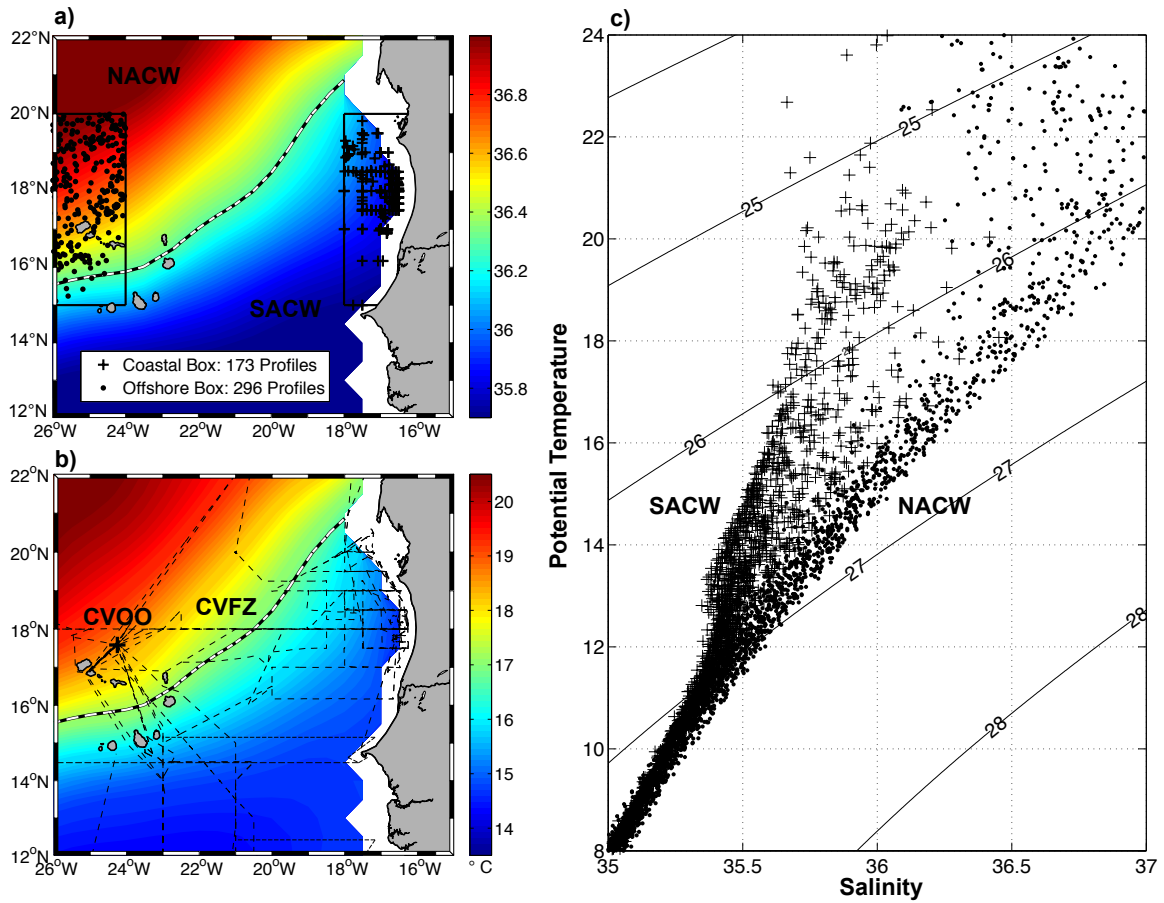
1 **Table 4:** Total available heat anomaly (AHA_{total}) and total available salt anomaly (ASA_{total}) of the composite
 2 cyclones, anticyclones and ACMEs as well as contribution of a single eddy to the annual heat and salt transport
 3 and its mean volume.
 4

	Cyclones	Anticyclones	ACMEs
AHA_{total} [x 10 ¹⁸ J]	-14.5	11.0	-15.4
ASA_{total} [x 10 ¹⁰ kg]	-73.0	40.7	-94.2
Heat transport [x 10 ¹¹ W]	-4.6	3.5	-4.9
Salt transport [x 10 ³ kg s ⁻¹]	-23.2	12.9	-29.9
Volume [x 10 ¹⁰ m ³]	286.0	308.9	297.3

1 Figures

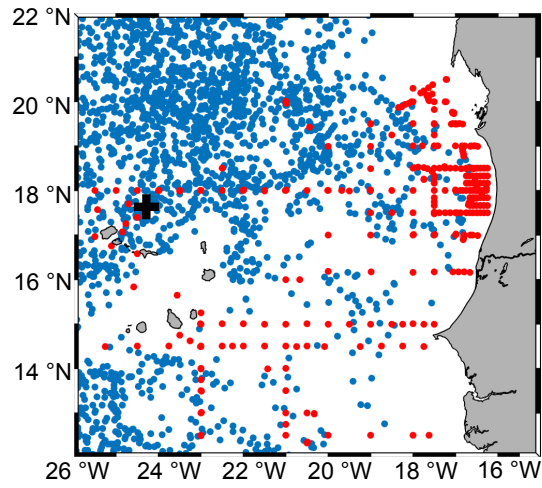


2
3
4 **Figure 1:** Schematic of the current system of the eastern tropical North Atlantic (red arrows; North Equatorial
5
6
7
8
9
10
Current (NEC), Canary Current (CC), Poleward Undercurrent (PUC), Mauretania Current (MC), North
Equatorial Countercurrent (nNECC), Guinea Current (GC), North Equatorial Undercurrent (NEUC))) **a)** in
boreal spring and **b)** in boreal autumn. Black arrows are mean wind vectors, green areas indicate seasonal mean
SST < 21°C. Blue colors represent topography and the dashed box indicates the TANWA area. The mean position
of the Intertropical Convergence Zone (ITCZ) in autumn is indicated as the region bounded by the two black
dashed lines in **b)**.



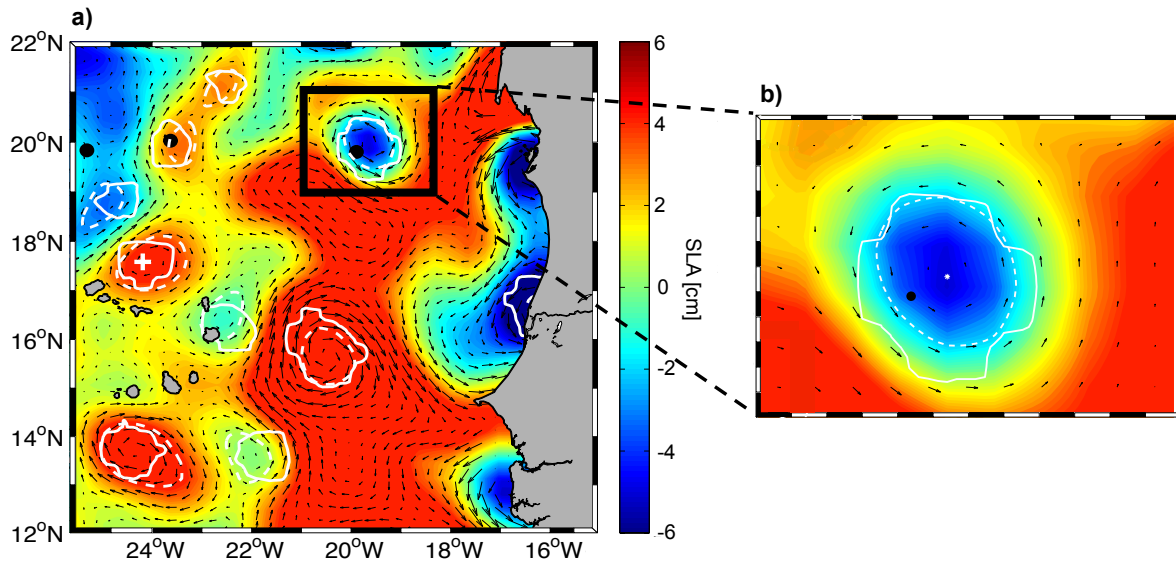
1

2 **Figure 2:** Mean salinity (a) and potential temperature (b) at 100 m depth in the TANWA from the MIMOC
 3 Climatology (Schmidtke et al., 2013) and θ/S diagram (c). The thick black/white line in a) and b) indicates the
 4 CVFZ. In a) crosses and dots represent all available profiles (from Argo floats and ships) in the marked coastal
 5 and offshore boxes, respectively. In b), the thin dashed line mark cruise tracks of 20 research cruises to the
 6 TANWA taking profiles used in the present study. The black cross in b) indicates the position of the Cape Verde
 7 Ocean Observatory (CVOO) mooring. In c) data from the coastal and offshore boxes are marked by crosses and
 8 dots, respectively; superimposed are isolines of potential density.
 9



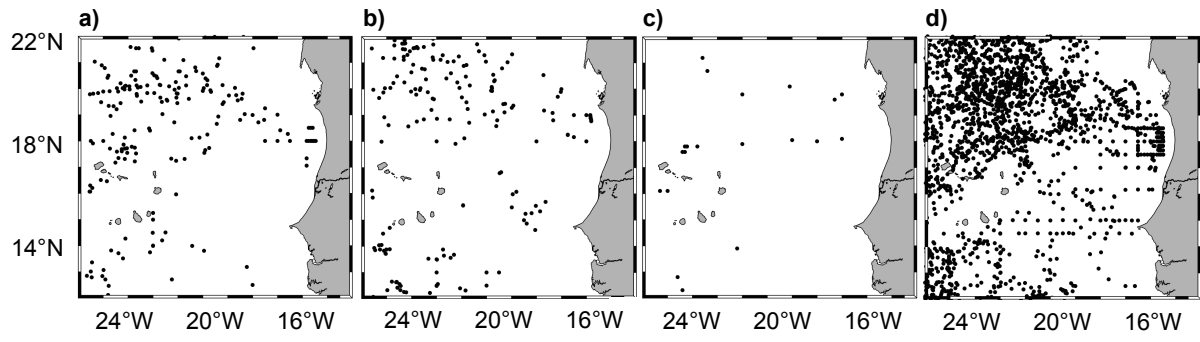
1

2 **Figure 3:** Locations of available temperature and salinity profiles obtained in the TANWA between 1995 and
3 2013. Red dots mark shipboard CTD stations, blue dots locations of Argo float profiles and the black cross the
4 location of the CVOO mooring.
5



1

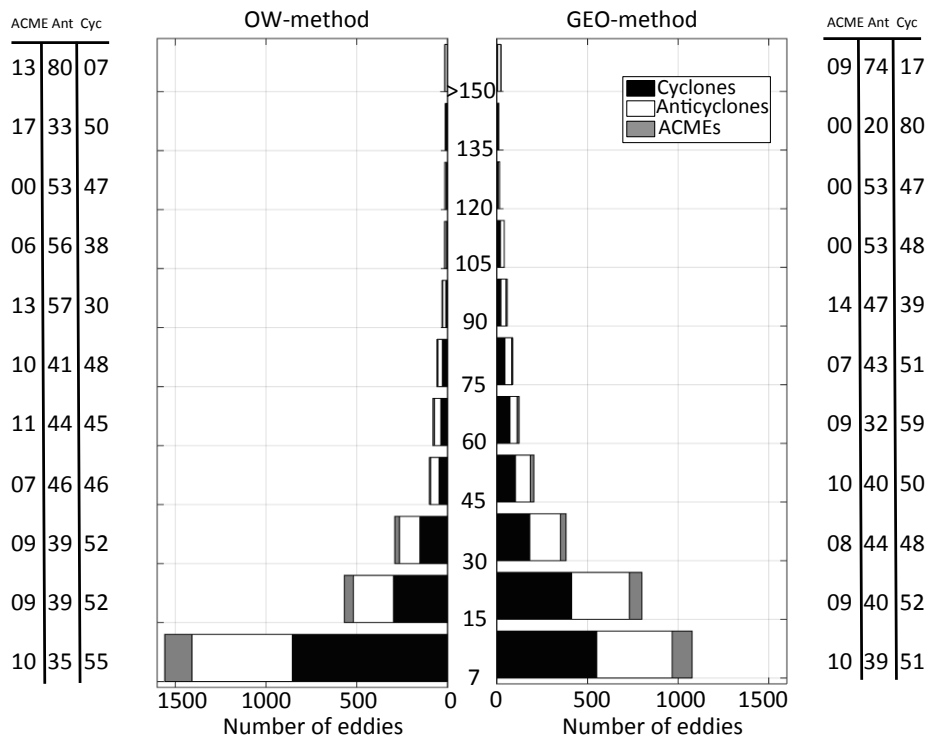
2 **Figure 4:** Snapshot of the SLA for Dec. 22, 2010, with the results of the eddy-detection methods: OW-Method
 3 (solid white line) and the GEO-Method (dashed white line) with geostrophic velocities superimposed (black
 4 arrows). The black dots mark Argo float profiles, the white cross in **a**) indicates the CVOO mooring. In **b**) a
 5 zoom of a selected region with a cyclonic eddy is shown.
 6



1

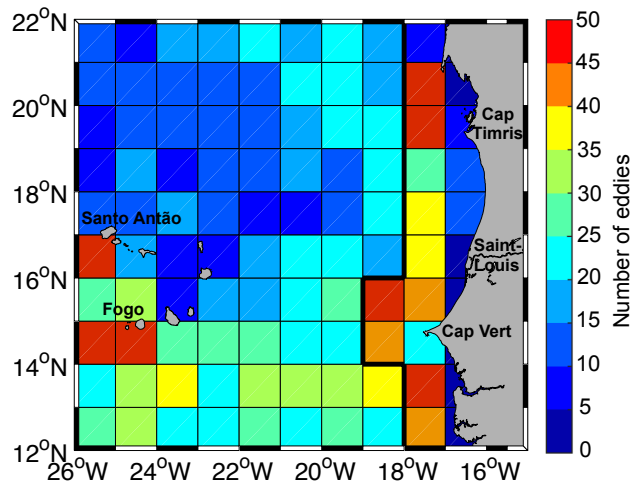
2
3

Figure 5: Location of all profiles taken in **a)** cyclones, **b)** anticyclones, **c)** ACMEs and **d)** outside of an eddy.



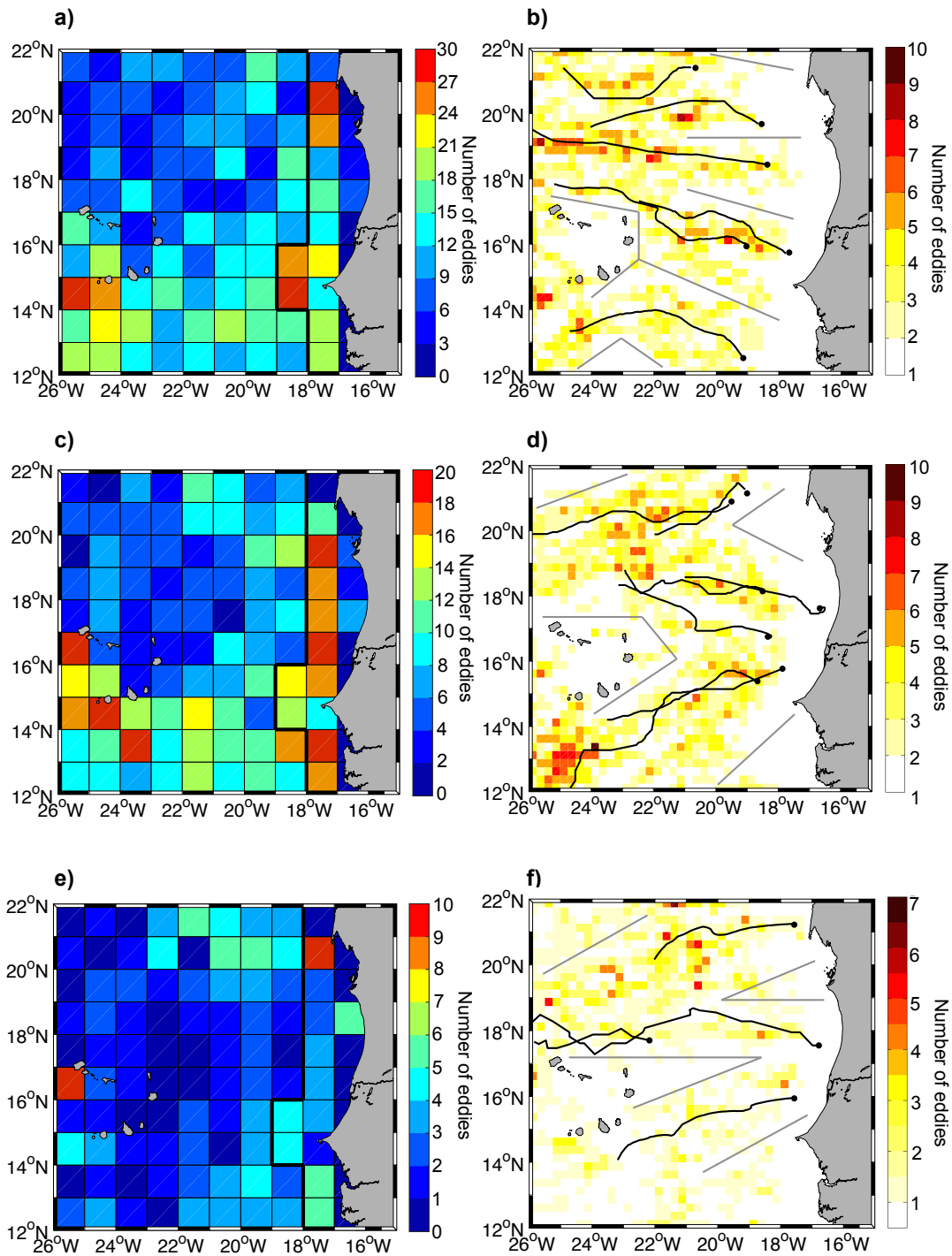
1

2 **Figure 6:** Number of eddies against lifetime in days from the OW-method (left) and GEO-method (right).
 3 Percentage of ACMEs, anticyclones (Ant) and cyclones (Cyc) is given in the tables on the right and left.
 4



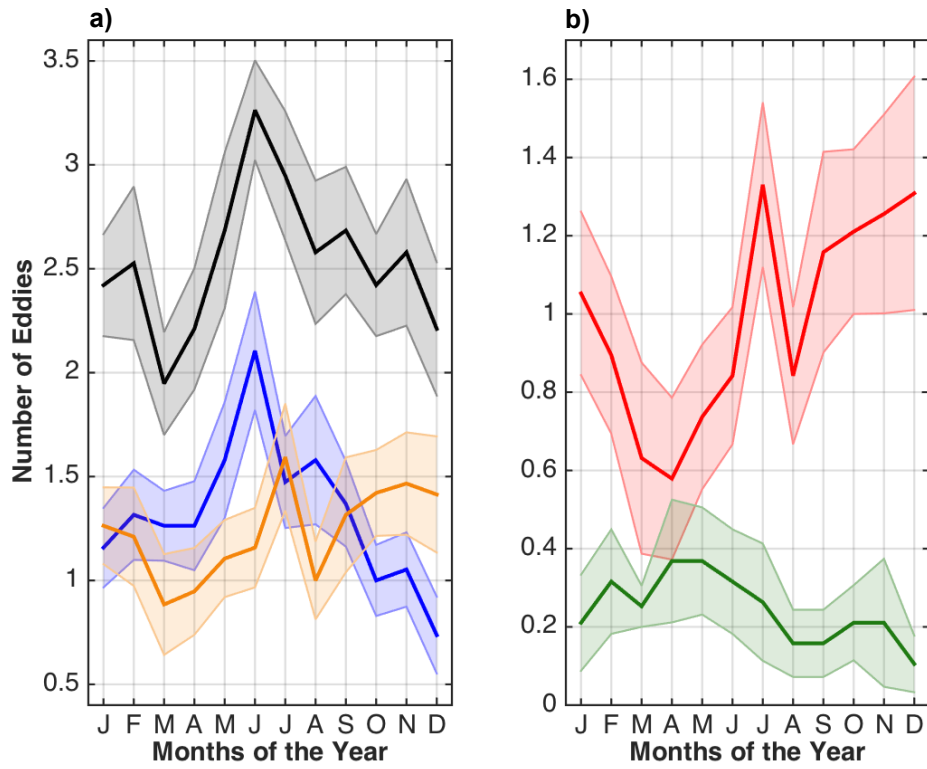
1

2 **Figure 7:** Number of eddies generated in 1° x 1° boxes (colors) between 1995 and 2013 based on the results of
 3 the OW-method. Marked are the headlands Cap Timiris (Mauretania), Saint-Louis (Senegal), Cap Vert (Senegal)
 4 and the Islands Santo Antão (Cape Verde) and Fogo (Cape Verde), which can be associated with high eddy
 5 generation. The thick solid black line along 18°W/19°W separates the coastal region from the offshore region.
 6



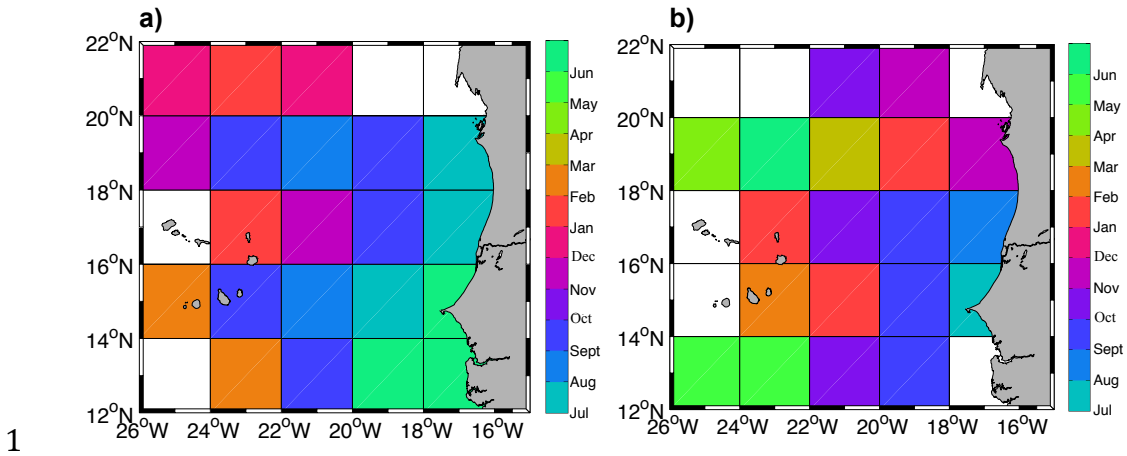
1

2 **Figure 8:** Number of eddies generated in $1^\circ \times 1^\circ$ boxes (a, c, e) and number of long-lived eddies detected in $1/6^\circ$
 3 $\times 1/6^\circ$ boxes based on the results of the OW-method (b, d, f) for cyclones (a, b), anticyclones (c, d) and ACMEs
 4 (e, f). In b), d) and f) only eddies are counted with a lifetime larger than 35 days. In b), d), and f) main eddy
 5 propagation corridors are indicated by straight gray lines; black lines show trajectories of long-lived eddies with
 6 a lifetime larger than 150 days. The thick solid black line along $18^\circ\text{W}/19^\circ\text{W}$ in a), c) and e) separates the coastal
 7 region from the offshore region.
 8



1

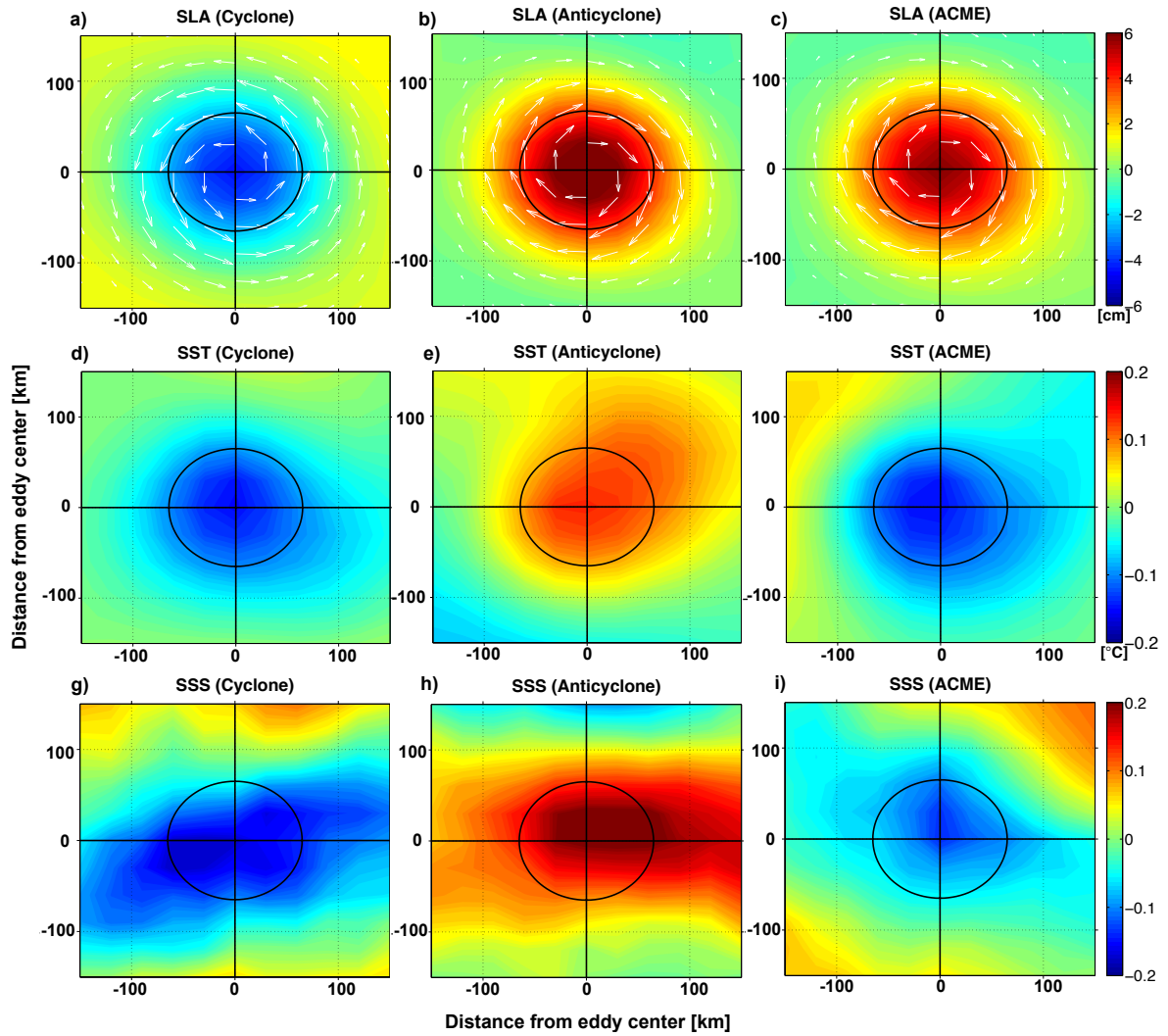
2 **Figure 9:** Seasonal cycle of the number of eddies generated in the coastal region per year based on the results of
 3 the OW-method as shown in Figures 7 and 8. In **a)** the seasonal cycle of all eddies is marked by the black line,
 4 of cyclones by the blue line and of all anticyclonic eddies by the orange line. In **b)** the seasonal cycle of
 5 anticyclonic eddies is separated into anticyclones (red line) and ACMEs (green line). The shaded areas around
 6 the lines represent the standard error.
 7



1

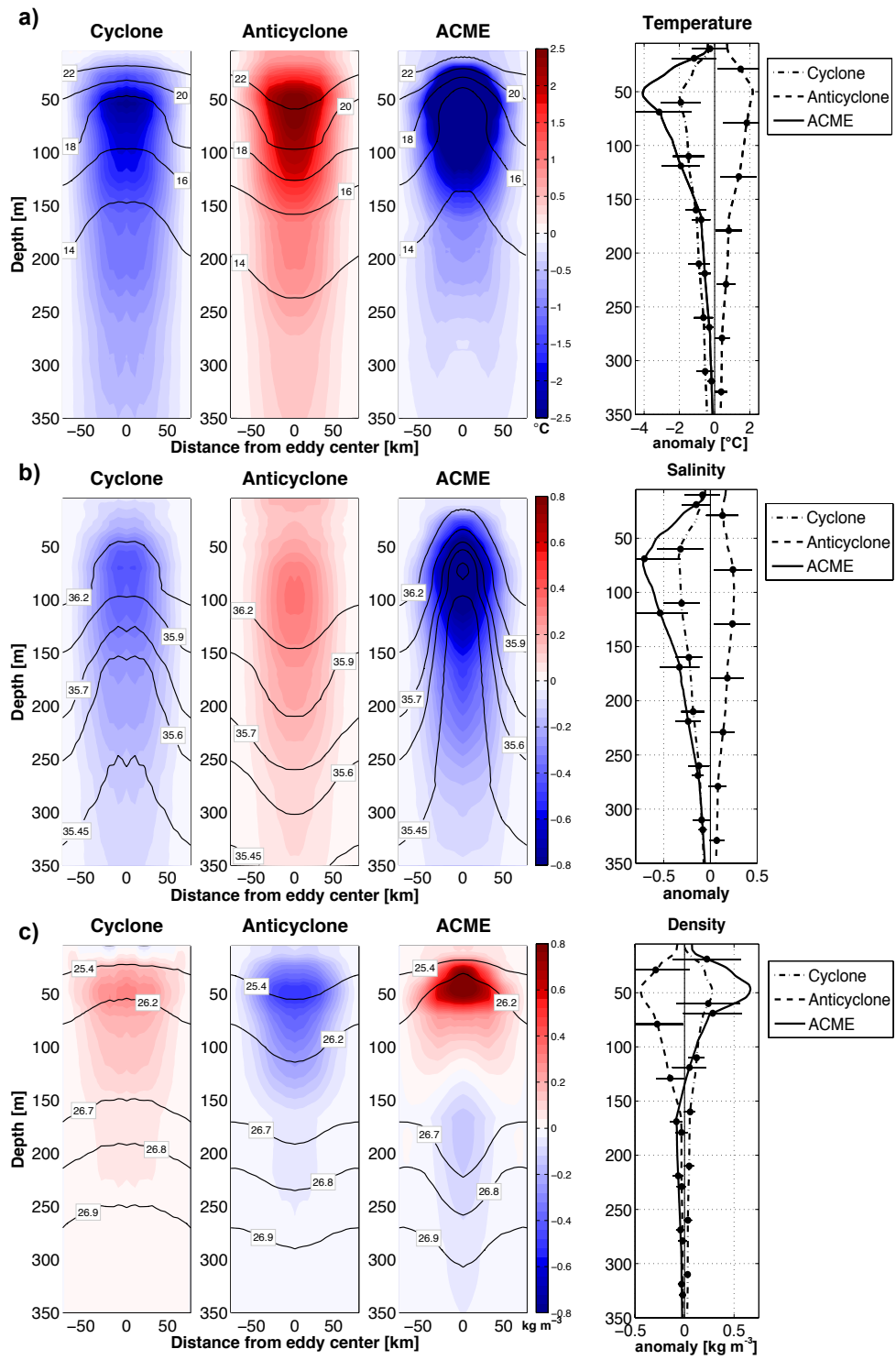
2
3
4
5

Figure 10: Phase of the annual harmonic of the number of detected eddies in $2^\circ \times 2^\circ$ boxes based on the results of the OW-method for **a)** cyclones and **b)** anticyclones. Phases are only shown for boxes with an amplitude larger than 2.5 eddies. Phase is given in month of the year with maximum eddy number.



1

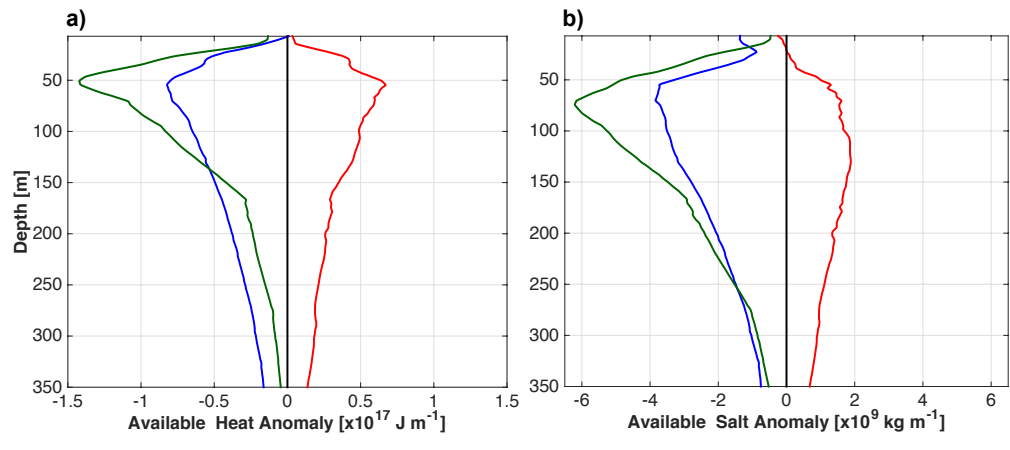
2 **Figure 11:** SLA, SST and SSS anomalies of the composite cyclone, anticyclone and ACME in the TANWA
 3 based on the results of the OW-method. SLA (color) and the associated geostrophic velocity (white arrows) are
 4 shown for each eddy type in **a)**, **b)** and **c)**; SST anomaly in **d)**, **e)** and **f)**; and SSS anomaly in **g)**, **h)** and **i)**,
 5 respectively. The circles mark the mean eddy radius.
 6



1

2
3
4
5
6
7
8
9

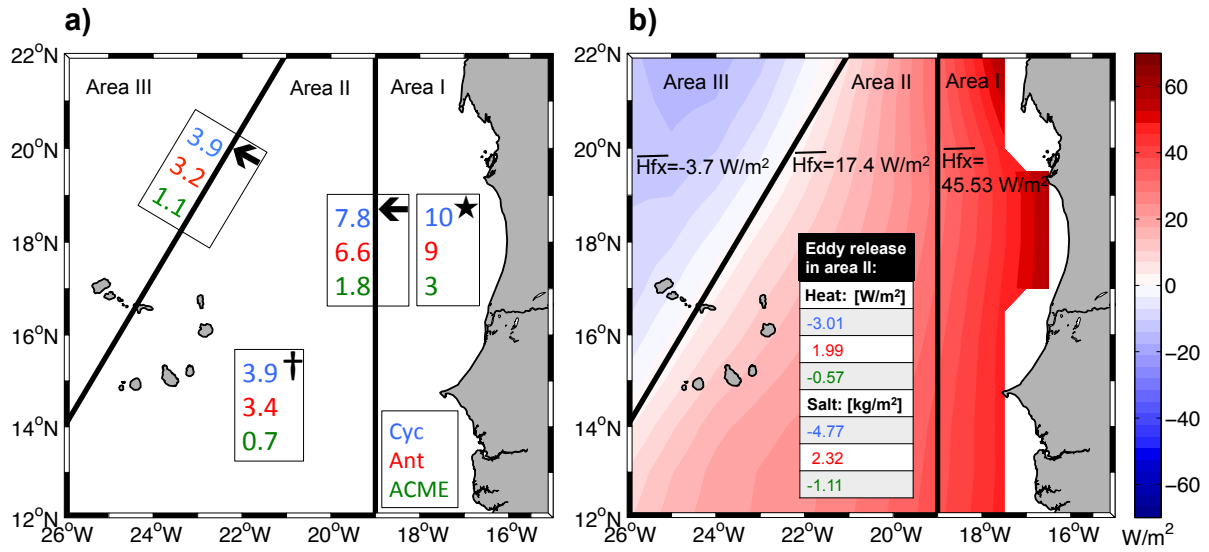
Figure 12: Vertical structure of the composite cyclone, anticyclone and ACME in the TANWA as presented as sections through the eddy center (left three columns) and mean anomaly profiles (right column). In **a**) potential temperature anomaly, in **b**) salinity anomaly and in **c**) potential density anomaly as calculated by using the nearest profile outside of the eddy is shown. Black contour lines in the left three columns mark isolines of temperature (**a**), salinity (**b**) and potential density (**c**). In the right column, solid lines represent the composite ACME, dashed lines the anticyclone and dashed-dotted lines the cyclone; the error bars at selected depths represent the standard deviation calculated from the individual anomaly profiles.



1

2
3
4

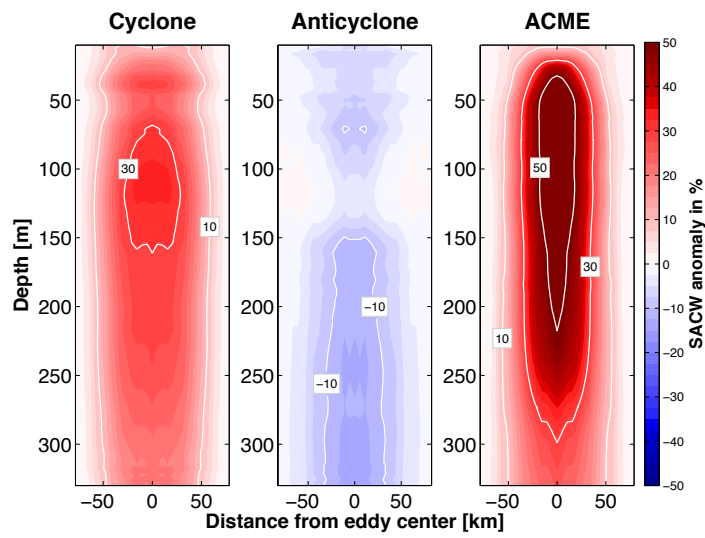
Figure 13: Mean profiles of available **a)** heat and **b)** salt anomaly per meter of the composite cyclone (blue line), anticyclone (red line) and ACME (green line).



1

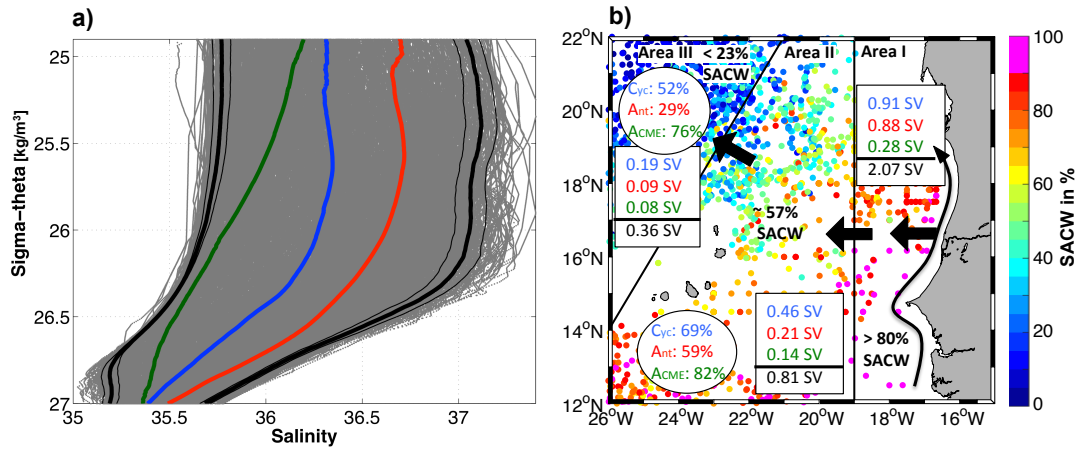
2 **Figure 14:** a) Map of the TANWA divided into three areas (Area I: the extended boundary current region, Area
 3 II: the transition zone, and Area III: the subtropical gyre region). Numbers inside of the boxes are the numbers of
 4 eddies (blue-cyclones, red-anticyclones, green-ACMEs), which are generated (star) and cease (cross) in an area
 5 or propagate from one area into another (arrow). b) Annual mean net heat flux from NOC Surface Flux Dataset
 6 (colors) with three areas marked. Black numbers are the area averaged net heat fluxes (\overline{Hfx}) in the
 7 corresponding areas. The table includes the eddy type dependent (blue: cyclones, red: anticyclones, green:
 8 ACMEs) heat and salt release in Area II.

9



1

2 **Figure 15:** Vertical sections of SACW anomaly through the center of the composite cyclone (left), anticyclone
 3 (middle) and ACME (right) in the TANWA.
 4



1

2 **Figure 16:** a) S- σ_θ diagram with thick and thin black lines indicating mean and standard deviation, respectively,
3 of characteristic SACW and NACW properties derived from the ensemble of profiles taken in the TANWA
4 (grey lines). Mean eddy dependent watermass properties are given for cyclones (blue line), anticyclones (red
5 line) and ACMEs (green line). b) Percentage of SACW in the upper 350m as shown for all available profiles
6 (color) and as mean numbers for the three regions: the extended boundary current region (Area I), the transition
7 zone (Area II) and the subtropical gyre region (Area III) that are separated by black straight lines. Numbers in
8 the white circles are the mean percentage of SACW of the composite cyclones (blue), anticyclones (red) and
9 ACMEs (green) in the corresponding areas. The eddy transport of SACW from the boundary current into Area I,
10 from Area I into Area II and from Area II into Area III is marked by thick black arrows with transport numbers
11 in Sv given in the white boxes for composite cyclones (blue), anticyclones (red), ACMEs (green) and total
12 transport (black).

References

- 1
2
3
4 Alpers, W., Brandt, P., Lazar, A., Dagherne, D., Sow, B., Faye, S., Hansen, M. W., Rubino, A.,
5 Poulain, P.-M., and Brehmer, P.: A small-scale oceanic eddy off the coast of West Africa
6 studied by multi-sensor satellite and surface drifter data, *Remote Sensing of*
7 *Environment*, 129, 132-143, 2013.
- 8 Barton, E.: Meanders, eddies and intrusions in the thermohaline front off Northwest
9 Africa, *Oceanol Acta*, 10, 267-283, 1987.
- 10 Barton, E. D.: The Poleward Undercurrent on the Eastern Boundary of the Subtropical
11 North Atlantic. In: *Poleward Flows Along Eastern Ocean Boundaries*, Neshyba, S. J.,
12 Mooers, C. N. K., Smith, R. L., and Barber, R. T. (Eds.), *Coastal and Estuarine Studies*,
13 Springer New York, 82-95, 1989.
- 14 Berry, D. I. and Kent, E. C.: Air–Sea fluxes from ICOADS: the construction of a new
15 gridded dataset with uncertainty estimates, *International Journal of Climatology*, 31,
16 987-1001, 2011.
- 17 Boutin, J., Martin, N., Reverdin, G., Yin, X., and Gaillard, F.: Sea surface freshening inferred
18 from SMOS and ARGO salinity: Impact of rain, *Ocean Sci*, 9, 183-192, 2013.
- 19 Brandt, P., Bange, H. W., Banyte, D., Dengler, M., Didwischus, S. H., Fischer, T., Greatbatch,
20 R. J., Hahn, J., Kanzow, T., Karstensen, J., Körtzinger, A., Krahnmann, G., Schmidtke, S.,
21 Stramma, L., Tanhua, T., and Visbeck, M.: On the role of circulation and mixing in the
22 ventilation of oxygen minimum zones with a focus on the eastern tropical North Atlantic,
23 *Biogeosciences*, 12, 489-512, 2015.
- 24 Chaigneau, A., Eldin, G., and Dewitte, B.: Eddy activity in the four major upwelling
25 systems from satellite altimetry (1992–2007), *Progress in Oceanography*, 83, 117-123,
26 2009.
- 27 Chaigneau, A., Gizolme, A., and Grados, C.: Mesoscale eddies off Peru in altimeter records:
28 Identification algorithms and eddy spatio-temporal patterns, *Progress in Oceanography*,
29 79, 106-119, 2008.
- 30 Chaigneau, A., Le Texier, M., Eldin, G., Grados, C., and Pizarro, O.: Vertical structure of
31 mesoscale eddies in the eastern South Pacific Ocean: A composite analysis from
32 altimetry and Argo profiling floats, *Journal of Geophysical Research: Oceans*, 116,
33 C11025, doi:10.1029/2011JC007134, 2011.
- 34 Chang, C.-H., Xie, S.-P., Schneider, N., Qiu, B., Small, J., Zhuang, W., Taguchi, B., Sasaki, H.,
35 and Lin, X.: East Pacific ocean eddies and their relationship to subseasonal variability in
36 Central American wind jets, *Journal of Geophysical Research: Oceans*, 117, C10001,
37 doi:10.1029/2011JC007315, 2012.

- 1 Chelton, D. B., deSzoeke, R. A., Schlax, M. G., El Naggar, K., and Siwertz, N.: Geographical
2 Variability of the First Baroclinic Rossby Radius of Deformation, *Journal of Physical*
3 *Oceanography*, 28, 433-460, 1998.
- 4 Chelton, D. B., Schlax, M. G., and Samelson, R. M.: Global observations of nonlinear
5 mesoscale eddies, *Progress in Oceanography*, 91, 167-216, 2011.
- 6 Chelton, D. B., Schlax, M. G., Samelson, R. M., and de Szoeke, R. A.: Global observations of
7 large oceanic eddies, *Geophysical Research Letters*, 34, L15606,
8 doi:10.1029/2007GL030812, 2007.
- 9 Crawford, W., Cherniawsky, J., Foreman, M., and Gower, J.: Formation of the Haida -
10 1998 oceanic eddy, *Journal of Geophysical Research: Oceans (1978–2012)*, 107, 6-1-6-
11 11, 2002.
- 12 Cushman Roisin B. and Tang B.: Geostrophic Turbulence and Emergence of Eddies
13 beyond the Radius of Deformation, *Journal of Physical Oceanography*, 20, 97–113, doi:
14 10.1175/15200485(1990)020<0097:GTAEOE>2.0.CO;2., 1990
15
- 16 Cushman-Roisin, B., Tang, B., and Chassignet, E. P.: Westward Motion of Mesoscale
17 Eddies, *Journal of Physical Oceanography*, 20, 758-768, 1990.
- 18 de Boyer Montégut, C., Madec, G., Fischer, A. S., Lazar, A., and Iudicone, D.: Mixed layer
19 depth over the global ocean: An examination of profile data and a profile-based
20 climatology, *Journal of Geophysical Research: Oceans*, 109, C12003,
21 doi:10.1029/2004JC002378, 2004.
- 22 Fu, L.-L. and Ferrari, R.: Observing Oceanic Submesoscale Processes From Space, *Eos*,
23 *Transactions American Geophysical Union*, 89, 488-488, 2008.
- 24 Garzoli, S. L. and Katz, E. J.: The Forced Annual Reversal of the Atlantic North Equatorial
25 Countercurrent, *Journal of Physical Oceanography*, 13, 2082-2090, 1983.
- 26 Glessmer, M. S., Eden, C., and Oschlies, A.: Contribution of oxygen minimum zone waters
27 to the coastal upwelling off Mauritania, *Progress in Oceanography*, 83, 143-150, 2009.
- 28 Hagen, E.: A meandering intermediate front North-West off Cape Verde islands, 1985.
29 *Oceanogr. Trop.*, 20: 71-83, 1985.
- 30 Hood, E.M.C, L. Sabine and B.M. Sloyan: The GO-SHIP repeat hydrography manual: A
31 collection of expert reports and guidelines, IOCCP Rep 14, 2010
- 32 Hughes P. and E. D. Barton: Stratification and water mass structure in the upwelling area
33 off Northwest Africa in April/May 1969, *Deep-Sea Research*, 21, 6111-628, 1974

- 1 Isern-Fontanet, J., García-Ladona, E., and Font, J.: Vortices of the Mediterranean Sea: An
2 Altimetric Perspective, *Journal of Physical Oceanography*, 36, 87-103, 2006.
- 3 Johns, W. E., Zantopp, R. J., and Goni, G. J.: Cross-gyre transport by North Brazil Current
4 rings, *Elsevier Oceanography Series*, 68, 411-441, 2003.
- 5 Jones, P. G. W. and A. R. Folkard: Chemical oceanographical observations off the coast of
6 North-West Africa, with special reference to the process of upwelling, *Rapports et*
7 *procès verbaux du Conseil International pour l'Exploration de la Mer* 159, 38-60, 1970
8
- 9 Karstensen, J., Fiedler, B., Schütte, F., Brandt, P., Körtzinger, A., Fischer, G., Zantopp, R.,
10 Hahn, J., Visbeck, M., and Wallace, D.: Open ocean dead zones in the tropical North
11 Atlantic Ocean, *Biogeosciences*, 12, 2597-2605, 2015.
- 12 Klinger, B. A.: Baroclinic eddy generation at a sharp corner in a rotating system, *Journal*
13 *of Geophysical Research: Oceans* (1978–2012), 99, 12515-12531, 1994a.
- 14 Klinger, B. A.: Inviscid Current Separation from Rounded Capes, *Journal of Physical*
15 *Oceanography*, 24, 1805-1811, 1994b.
- 16 Kostianoy, A. G. and Belkin, I. M.: A Survey of Observations on Emtrathermocline Eddies
17 in the World Ocean. In: *Elsevier Oceanography Series*, Nihoul, J. C. J. and Jamart, B. M.
18 (Eds.), Elsevier, 1989.
- 19 Kurczyn, J., Beier, E., Lavín, M., and Chaigneau, A.: Mesoscale eddies in the northeastern
20 Pacific tropical - subtropical transition zone: Statistical characterization from satellite
21 altimetry, *Journal of Geophysical Research: Oceans* (1978–2012), 117, C10021,
22 doi:10.1029/2012JC007970, 2012.
- 23 Kurian, J., Colas, F., Capet, X., McWilliams, J. C., and Chelton, D. B.: Eddy properties in the
24 California current system, *Journal of Geophysical Research: Oceans* (1978–2012), 116,
25 C08027, doi:10.1029/2010JC006895, 2011.
- 26 Lázaro, C., Fernandes, M. J., Santos, A. M. P., and Oliveira, P.: Seasonal and interannual
27 variability of surface circulation in the Cape Verde region from 8 years of merged T/P
28 and ERS-2 altimeter data, *Remote Sensing of Environment*, 98, 45-62, 2005.
- 29 Liang, J.-H., McWilliams, J. C., Kurian, J., Colas, F., Wang, P., and Uchiyama, Y.: Mesoscale
30 variability in the northeastern tropical Pacific: Forcing mechanisms and eddy properties,
31 *Journal of Geophysical Research: Oceans*, 117, C07003, doi: 10.1029/2012JC008008,
32 2012.
- 33 Liu Y., C. Dong, Y. Guan, D. Chen, J. McWilliams, F. Nencioli: Eddy analysis in the
34 subtropical zonal band of the North Pacific Ocean, *Deep Sea Research Part I:*
35 *Oceanographic Research Papers*, Volume 68, Pages 54-67, ISSN 0967-0637,
36 <http://dx.doi.org/10.1016/j.dsr.2012.06.001>, 2012

- 1
- 2 Luyten, J. R., Pedlosky, J., and Stommel, H.: The ventilated thermocline, *Journal of*
3 *Physical Oceanography*, 13, 292-309, 1983.
- 4 Mittelstaedt, E.: The ocean boundary along the Northwest African Coast - circulation and
5 oceanographic properties at the sea-surface, *Progress in Oceanography*, 26, 307-355,
6 1991.
- 7 Mittelstaedt, E.: The upwelling area off Northwest Africa - a description of phenomena
8 related to coastal upwelling, *Progress in Oceanography*, 12, 307-331, 1983.
- 9 Nencioli, F., Dong, C., Dickey, T., Washburn, L., and McWilliams, J. C.: A Vector Geometry-
10 Based Eddy Detection Algorithm and Its Application to a High-Resolution Numerical
11 Model Product and High-Frequency Radar Surface Velocities in the Southern California
12 Bight, *J Atmos Ocean Tech*, 27, 564-579, 2010.
- 13 Okubo, A.: Horizontal dispersion of floatable particles in the vicinity of velocity
14 singularities such as convergences, *Deep Sea Research and Oceanographic Abstracts*, 17,
15 445-454, 1970.
- 16 Ould-Dedah, S., Wiseman Jr, W. J., and Shaw, R. F.: Spatial and temporal trends of sea
17 surface temperature in the northwest African region, *Oceanol Acta*, 22, 265-279, 1999.
- 18 Pantoja, D., Marinone, S., Parés-Sierra, A., and Gómez-Valdivia, F.: Numerical modeling of
19 seasonal and mesoscale hydrography and circulation in the Mexican Central Pacific
20 Modelación numérica de la hidrografía y circulación estacional y de mesoescala en el
21 Pacífico central mexicano, *Ciencias Marinas*, 38, 363-379, 2012.
- 22 Pares-Sierra, A., White, W. B., and Tai, C. K.: Wind-driven Coastal Generation of Annual
23 Mesoscale Eddy Activity in the California Current, *Journal of Physical Oceanography*, 23,
24 1110-1121, 1993.
- 25 Pastor, M. V., Pelegrí, J. L., Hernández-Guerra, A., Font, J., Salat, J., and Emelianov, M.:
26 Water and nutrient fluxes off Northwest Africa, *Continental Shelf Research*, 28, 915-936,
27 2008.
- 28 Pegliasco C., Chaigneau A., Morrow R.: Main eddy vertical structures observed in the four
29 major Eastern Boundary Upwelling Systems, *Journal of Geophysical Research*, Vol. 120,
30 6008-6033, doi: 10.1002/2015JC01950, 2015
- 31 Peña-Izquierdo, J., Pelegrí, J. L., Pastor, M. V., Castellanos, P., Emelianov, M., Gasser, M.,
32 Salvador, J., and Vázquez-Domínguez, E.: The continental slope current system between
33 Cape Verde and the Canary Islands, *Sci Mar*, 76, 65-78, 2012.
- 34 Peña - Izquierdo, J., van Sebille, E., Pelegrí, J. L., Sprintall, J., Mason, E., Llanillo, P. J., and
35 Machín, F.: Water mass pathways to the North Atlantic oxygen minimum zone, *Journal of*

- 1 Geophysical Research: Oceans, vol. 120, page range 3350-3372,
2 doi:10.1002/2014JC010557, 2015.
- 3 Pichevin, T. and Nof, D.: The eddy cannon, Deep Sea Research Part I: Oceanographic
4 Research Papers, 43, 1475-1507, 1996.
- 5 Polonsky, A. and Artamonov, Y.: North equatorial countercurrent in the tropical Atlantic:
6 Multi-jet structure and seasonal variability, Deutsche Hydrographische Zeitschrift, 49,
7 477-495, 1997.
- 8 Richardson, P. L. and Reverdin, G.: Seasonal cycle of velocity in the Atlantic North
9 Equatorial Countercurrent as measured by surface drifters, current meters, and ship
10 drifts, Journal of Geophysical Research: Oceans, 92, 3691-3708, 1987.
- 11 Røed, L. P.: Curvature effects on hydraulically driven inertial boundary currents, J Fluid
12 Mech, 96, 395-412, 1980.
- 13 Sangrà, P., Pascual, A., Rodríguez-Santana, Á., Machín, F., Mason, E., McWilliams, J. C.,
14 Pelegrí, J. L., Dong, C., Rubio, A., Arístegui, J., Marrero-Díaz, Á., Hernández-Guerra, A.,
15 Martínez-Marrero, A., and Auladell, M.: The Canary Eddy Corridor: A major pathway for
16 long-lived eddies in the subtropical North Atlantic, Deep Sea Research Part I:
17 Oceanographic Research Papers, 56, 2100-2114, 2009.
- 18 Schmidtko, S., Johnson, G. C., and Lyman, J. M.: MIMOC: A global monthly isopycnal
19 upper-ocean climatology with mixed layers, Journal of Geophysical Research: Oceans,
20 118, 1658-1672, 2013.
- 21 Siedler, G., Zangenberg, N., Onken, R., and Morlière, A.: Seasonal changes in the tropical
22 Atlantic circulation: Observation and simulation of the Guinea Dome, Journal of
23 Geophysical Research: Oceans, 97, 703-715, 1992.
- 24 Stramma, L., Bange, H. W., Czeschel, R., Lorenzo, A., and Frank, M.: On the role of
25 mesoscale eddies for the biological productivity and biogeochemistry in the eastern
26 tropical Pacific Ocean off Peru, Biogeosciences, 10, 7293-7306, 2013.
- 27 Stramma, L. and Isemer, H.-J.: Seasonal variability of meridional temperature fluxes in
28 the eastern North Atlantic Ocean, J Mar Res, 46, 281-299, 1988.
- 29 Stramma, L. and Schott, F.: The mean flow field of the tropical Atlantic Ocean, Deep Sea
30 Research Part II: Topical Studies in Oceanography, 46, 279-303, 1999.
- 31 Stramma, L. and Siedler, G.: Seasonal changes in the North Atlantic subtropical gyre,
32 Journal of Geophysical Research: Oceans, 93, 8111-8118, 1988.
- 33 Weiss, J.: The dynamics of enstrophy transfer in two-dimensional hydrodynamics,
34 Physica D: Nonlinear Phenomena, 48, 273-294, 1991.

- 1 Yin, X., Boutin, J., and Spurgeon, P.: First assessment of SMOS data over open ocean: Part
2 I—Pacific Ocean, *Geoscience and Remote Sensing, IEEE Transactions on*, 50, 1648-1661,
3 2012.
- 4 Zamudio, L., Hurlburt, H. E., Metzger, E. J., Morey, S. L., O'Brien, J. J., Tilburg, C., and
5 Zavala - Hidalgo, J.: Interannual variability of Tehuantepec eddies, *Journal of*
6 *Geophysical Research: Oceans* (1978–2012), 111, C05001, doi:10.1029/2005JC003182,
7 2006.
- 8 Zamudio, L., Hurlburt, H. E., Metzger, E. J., and Tilburg, C. E.: Tropical wave - induced
9 oceanic eddies at Cabo Corrientes and the María Islands, Mexico, *Journal of Geophysical*
10 *Research: Oceans* (1978–2012), 112, C05048, doi:10.1029/2006JC004018, 2007.
- 11 Zamudio, L., Leonardi, A. P., Meyers, S. D., and O'Brien, J. J.: ENSO and eddies on the
12 southwest coast of Mexico, *Geophysical Research Letters*, 28, 13-16, 2001.
- 13 Zenk, W., Klein, B., and Schroder, M.: Cape Verde Frontal Zone, *Deep Sea Research Part A.*
14 *Oceanographic Research Papers*, 38, Supplement 1, S505-S530, 1991.
- 15 Zhang, Z., Wang, W., and Qiu, B.: Oceanic mass transport by mesoscale eddies, *Science*,
16 345, 322-324, 2014.
17
18